Geochemical Journal, Vol. 50, pp. 557 to 573, 2016 doi:10.2343/geochemj.2.0431

Discovery of extremely REY-rich mud in the western North Pacific Ocean

Koichi Iijima,[1] Kazutaka Yasukawa,[2,3] Koichiro Fujinaga,[3,4] Kentaro Nakamura,[2] Shiki Machida,[1] Yutaro Takaya,[5] Junichiro Ohta,[6] Satoru Haraguchi,[6] Yoshiro Nishio,[7] Yoichi Usui,[1] Tatsuo Nozaki,[1,4,8] Toshitsugu Yamazaki,[9,10] Yuji Ichiyama,[11] Akira Ijiri,[12,1] Fumio Inagaki,[12,1] Hideaki Machiyama,[1] Katsuhiko Suzuki,[1] Yasuhiro Kato[4,3,2,1]* and KR13-02 Cruise Members

[1]Research and Development Center for Submarine Resources, Japan Agency for Marine-Earth Science and Technology (JAMSTEC), 2-15 Natsushima-cho, Yokosuka, Kanagawa 237-0061, Japan
[2]Department of Systems Innovation, School of Engineering, The University of Tokyo, 7-3-1 Hongo, Bunkyo-ku, Tokyo 113-8656, Japan
[3]Ocean Resources Research Center for Next Generation, Chiba Institute of Technology, 2-17-1 Tsudanuma, Narashino, Chiba 275-0016, Japan
[4]Frontier Research Center for Energy and Resources, School of Engineering, The University of Tokyo, 7-3-1 Hongo, Bunkyo-ku, Tokyo 113-8656, Japan
[5]Department of Resources and Environmental Engineering, School of Creative Science and Engineering, Waseda University, 3-4-1 Okubo, Shinjyuku-ku, Tokyo 169-8555, Japan
[6]Department of Solid Earth Geochemistry, JAMSTEC, 2-15 Natsushima-cho, Yokosuka, Kanagawa 237-0061, Japan
[7]Department of Marine Resource Sciences, Faculty of Agriculture and Marine Science, Kochi University, 200 Monobe Otsu, Nankoku, Kochi 783-8502, Japan
[8]Department of Planetology, Graduate School of Science, Kobe University, 1-1 Rokkodai-cho, Nada-ku, Kobe, Hyogo 657-8501, Japan
[9]Department of Ocean Floor Geoscience, Atmosphere and Ocean Research Institute, The University of Tokyo, 5-1-5 Kashiwanoha, Kashiwa, Chiba 277-8564, Japan
[10]Geological Survey of Japan, National Institute of Advanced Industrial Science and Technology, 1-1-1 Higashi, Tsukuba, Ibaraki 305-8561, Japan
[11]Department of Earth Sciences, Faculty of Science, Chiba University, 1-33 Yayoi-cho, Inage-ku, Chiba 263-8522, Japan
[12]Kochi Institute for Core Sample Research, JAMSTEC, 200 Monobe Otsu, Nankoku, Kochi 783-8502, Japan

(*Received March 31, 2015; Accepted June 25, 2016*)

We have discovered deep-sea mud that is extremely enriched in rare-earth elements and yttrium (together called REY) in the Japanese Exclusive Economic Zone around Minamitorishima Island, in the western North Pacific Ocean. The maximum total REY concentration reaches approximately 7000 ppm, which is much higher than that reported for conventional REY deposits on land and other known potential REY resources in the ocean. The extremely REY-rich mud is characterized by abundant phillipsite and biogenic calcium phosphate. In addition, the stratigraphic layer with the highest REY concentration occurs just ~3 m beneath the seafloor. The shallow burial of these strata together with the high REY content, especially those of heavy rare-earth elements, suggest that the newly discovered extremely REY-rich mud may be a promising REY resource.

Keywords: extremely REY-rich mud, rare-earth elements, deep-sea mineral resources, Minamitorishima Island, western North Pacific Ocean

Introduction

Modern society has increasingly become dependent on high-tech devices, such as personal computers, smartphones, and flat-screen televisions. The advancement of green technologies, including electric and hybrid vehicles, compact and long-life LED lights, and wind power generation, is required to shift human society toward sustainable growth. Rare-earth elements and yttrium, hereinafter together called REY, are essential elements for products with these advanced and green technologies, because of the magnetic and optical properties of REY that result from the characteristic configurations of electrons in these elements. With rising economic growth in

*Corresponding author (e-mail: ykato@sys.t.u-tokyo.ac.jp)

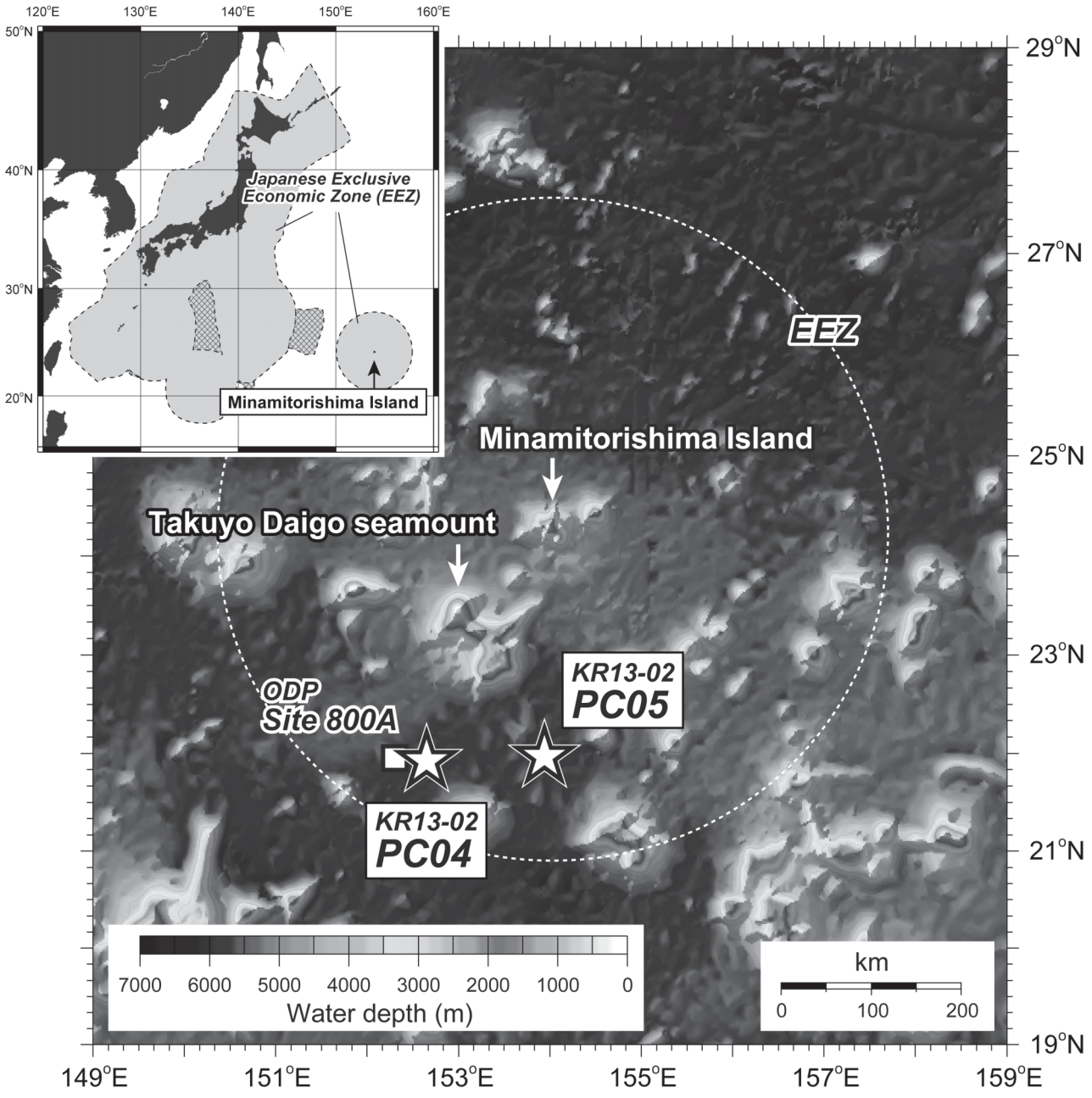

Fig. 1. Locations of KR13-02 PC04 and PC05. Bathymetric data are from ETOPO1 (NOAA's National Centers for Environmental Information (NCEI); https://www.ngdc.noaa.gov/mgg/global/global.html).

developing nations, the global demand of REY is forecast to grow rapidly (Alonso *et al*., 2012).

Kato *et al*. (2011) reported deep-sea mud in the Pacific Ocean that contains high concentrations of REY and proposed that they may be a viable new REY resource. We analyzed two drill cores recovered by the Deep Sea Drilling Project and the Ocean Drilling Program, and confirmed the presence of REY-rich mud in the Japanese Exclusive Economic Zone (EEZ) surrounding Minamitorishima Island, ~1900 km southeast of Tokyo in the western North Pacific Ocean (Kato *et al*., 2012).

In order to understand the spatial distribution of REY-rich mud in the Minamitorishima EEZ in more detail, new research cruises were recently conducted (Fujinaga *et al*., 2016; Nakamura *et al*., 2016). Here we focus on the discovery of anomalously REY-enriched layers in two piston cores (PC04 and PC05) collected during cruise KR13-02. Whereas typical REY-rich mud previously reported

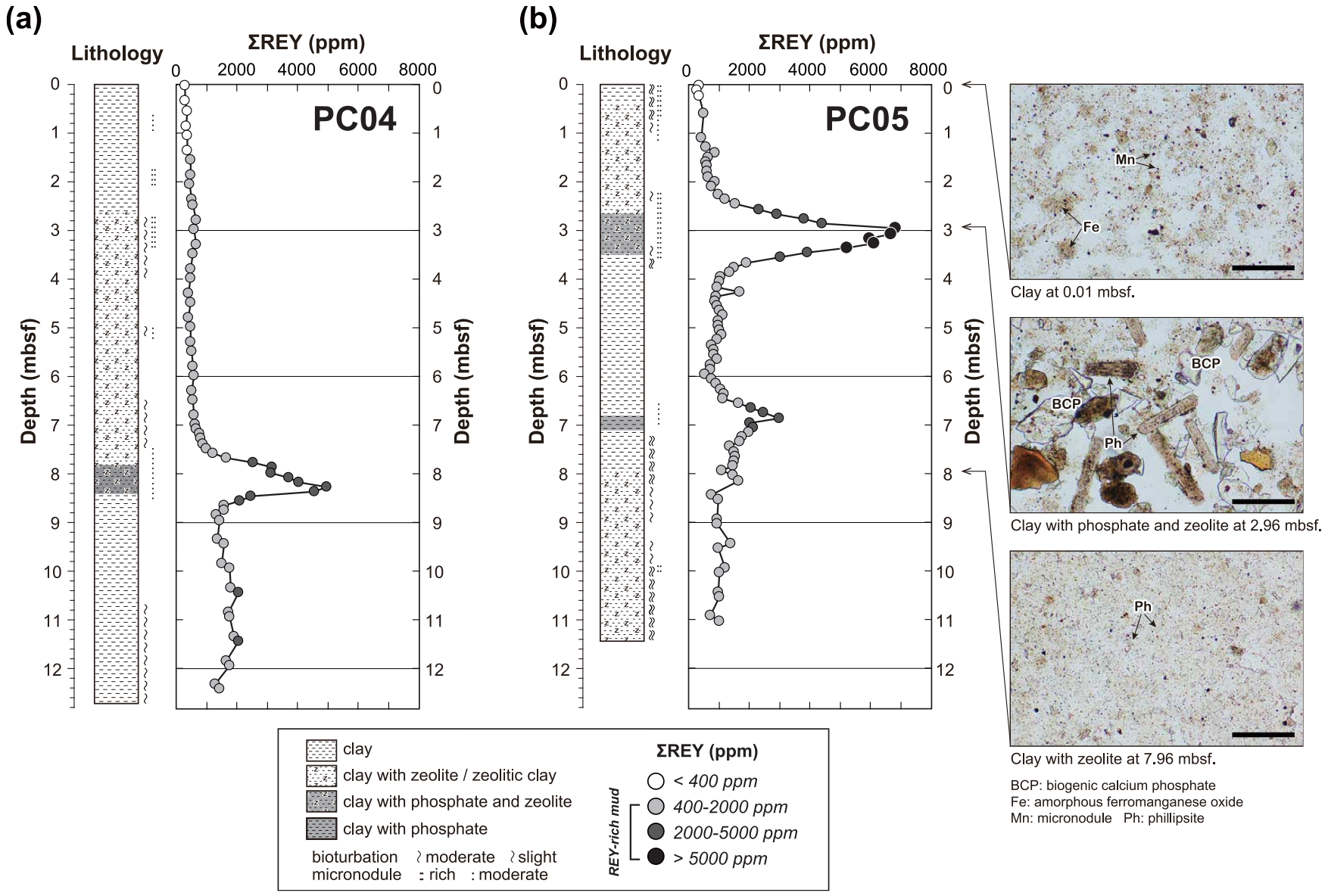

Fig. 2. Lithologic columns and depth profiles of ΣREY content for (a) PC04 and (b) PC05. Photomicrographs of representative smear-slide samples from PC05 are also shown in (b). Scale bar width represents 50 μm and height represents 4 μm.

Table 1. Major, trace, and rare-earth element data of KR13-02 PC04

Core	PC04	PC04	PC04	PC04	PC04	PC04	PC04	PC04	PC04	PC04	PC04	PC04	PC04	PC04	PC04
Section	1	1	2	2	2	2	3	3	3	3	4	4	4	4	5
Interval [cm]	2–4	32–34	2–4	32–34	52–54	82–84	2–4	32–34	52–54	82–84	2–4	32–34	52–54	82–84	2–4
Depth [mbsf]	0.03	0.33	0.55	0.85	1.05	1.35	1.56	1.86	2.06	2.36	2.50	2.80	3.00	3.30	3.49
SiO_2 (wt.%)	52.7	53.0	52.4	52.8	52.4	52.4	51.3	51.2	50.3	51.0	50.4	50.7	49.5	50.2	49.4
TiO_2	0.85	0.86	0.91	0.87	0.87	0.92	0.90	0.93	0.92	0.94	0.93	0.89	0.85	0.88	0.90
Al_2O_3	16.6	16.6	16.9	16.6	16.8	16.7	16.9	16.8	16.9	16.9	16.9	16.5	16.6	16.8	16.8
Fe_2O_3*	8.14	8.41	8.78	8.45	8.52	8.71	9.00	9.39	9.11	9.26	9.22	9.07	8.49	8.80	9.00
MnO	0.68	0.77	0.90	0.82	0.78	1.02	1.17	1.20	1.11	1.17	1.07	1.16	1.17	1.30	1.34
MgO	3.35	3.22	3.37	3.28	3.27	3.42	3.24	3.43	3.25	3.34	3.17	3.15	2.97	3.08	2.99
CaO	1.81	1.41	1.53	1.50	1.47	1.50	1.77	1.46	1.64	1.70	1.95	1.78	2.20	1.75	1.95
Na_2O	3.71	3.42	3.17	3.59	3.69	3.72	3.23	3.64	3.84	3.83	3.55	4.11	4.76	4.54	4.03
K_2O	3.24	3.34	3.39	3.34	3.37	3.40	3.21	3.28	3.29	3.24	3.18	3.21	3.47	3.33	3.23
P_2O_5	0.25	0.25	0.31	0.29	0.26	0.36	0.46	0.48	0.47	0.52	0.55	0.62	0.65	0.58	0.61
LOI	8.63	8.75	8.40	8.54	8.62	7.85	8.89	8.19	9.16	8.16	9.09	8.80	9.37	8.78	9.68
Total	100	100	100	100	100	100	100	100	100	100	100	100	100	100	100
La (ppm)	44.6	43.8	54.3	47.7	52.7	51.0	73.2	65.0	67.7	73.2	80.9	90.4	86.8	89.9	77.7
Ce	101	102	106	101	112	97.7	112	106	101	106	104	122	108	131	110
Pr	11.6	12.1	14.3	13.4	13.7	14.5	19.4	18.7	18.1	21.0	21.7	25.6	23.3	25.7	20.5
Nd	45.2	47.9	56.6	52.8	54.2	58.0	79.7	77.3	74.0	87.2	90.3	108	97.4	109	86.5
Sm	9.80	10.6	12.5	11.6	11.7	13.1	17.6	17.3	16.4	19.5	20.3	24.9	22.1	24.9	19.6
Eu	2.23	2.51	2.94	2.79	2.72	3.12	4.31	4.28	4.02	4.85	5.06	6.29	5.64	6.39	5.01
Gd	9.46	10.6	12.7	11.9	11.8	13.7	19.1	19.2	18.2	21.7	22.9	28.7	25.7	29.1	22.9
Tb	1.45	1.62	1.93	1.82	1.78	2.10	2.92	2.90	2.75	3.36	3.50	4.46	3.92	4.48	3.48
Dy	8.84	10.0	12.0	11.4	10.9	13.2	18.5	18.6	17.4	21.3	22.1	28.4	24.9	28.8	22.3
Ho	1.77	2.04	2.43	2.31	2.20	2.70	3.82	3.82	3.58	4.42	4.61	5.98	5.31	6.07	4.69
Er	5.07	6.04	7.00	6.75	6.48	7.89	11.2	11.1	10.4	12.9	13.4	17.5	15.4	17.4	13.7
Tm	0.73	0.84	0.99	0.97	0.92	1.11	1.59	1.57	1.47	1.82	1.90	2.48	2.19	2.49	1.92
Yb	4.73	5.52	6.49	6.27	6.03	7.13	10.3	10.00	9.48	11.5	12.3	15.7	14.0	15.9	12.5
Lu	0.74	0.85	1.02	0.96	0.94	1.12	1.63	1.59	1.45	1.82	1.91	2.49	2.20	2.49	1.95
Y	51.7	51.3	74.7	61.3	63.2	73.3	119	106	107	123	141	173	167	172	148
∑REY (ppm)	299	307	366	333	351	360	494	463	454	514	546	655	604	665	550
∑LREE	214	218	247	229	247	237	306	289	282	312	322	377	343	387	319
∑HREE	84.5	88.8	119	104	104	122	188	174	172	202	223	278	261	278	231
Ce/Ce*	1.01	1.01	0.87	0.91	0.95	0.82	0.68	0.70	0.67	0.62	0.57	0.58	0.55	0.62	0.63
Sc (ppm)	22.6	20.3	25.4	21.1	23.6	20.9	26.4	25.3	24.1	26.1	26.9	32.4	28.4	35.6	29.0
V	161	168	168	170	167	165	165	183	163	181	159	187	150	200	148
Cr	83.9	84.0	80.9	82.7	85.4	72.3	67.3	60.6	62.4	48.0	55.3	57.4	42.8	48.1	37.7
Co	73.4	73.4	94.1	81.0	80.7	88.7	121	118	107	113	113	141	132	163	150
Ni	139	119	175	135	145	145	214	214	242	194	223	237	250	218	234
Cu	226	205	274	228	238	235	317	318	314	307	334	363	332	374	329
Zn	142	129	161	136	149	139	168	162	164	162	167	181	162	184	158
Rb	135	124	143	126	146	120	132	118	112	108	103	98.4	97.3	94.8	87.4
Sr	191	178	203	188	198	189	225	203	194	223	225	245	211	255	214
Zr	123	125	142	127	136	131	155	160	152	165	159	190	157	192	152
Nb	14.7	13.9	16.7	14.4	16.1	14.2	16.6	15.4	15.8	16.4	15.1	15.4	13.8	15.0	12.7
Mo	9.87	18.5	22.0	19.7	19.2	25.1	35.6	35.7	37.3	47.0	45.3	54.6	54.3	75.2	68.5
Ba	587	541	497	533	582	448	429	437	367	381	357	391	321	381	296
Hf	2.76	3.15	2.99	3.16	3.19	3.17	3.43	3.91	3.29	3.99	3.62	4.56	3.47	4.74	3.44
Ta	0.95	1.02	0.99	1.03	1.08	0.97	0.98	1.01	0.95	1.02	0.87	0.91	0.76	0.89	0.69
Pb	34.4	39.8	40.0	40.5	42.0	39.6	46.0	45.8	41.0	44.1	40.5	44.4	39.5	48.9	41.5
Th	13.3	14.0	13.6	13.8	14.7	12.9	14.1	12.8	12.0	12.7	11.7	12.8	10.8	12.5	9.78
U	2.31	2.49	2.50	2.49	2.67	2.42	2.68	2.63	2.53	2.70	2.59	2.94	2.62	3.13	2.56

from the Pacific Ocean contains at most 2200 ppm of total REY (∑REY) (Kato *et al.*, 2011), the maximum ∑REY content of the mud in the Minamitorishima EEZ approaches nearly 7000 ppm, which suggests a highly promising new REY resource.

Core Descriptions and Analytical Methods

Cruise KR13-02 by *R/V Kairei* was conducted by the Japan Agency of Marine-Earth Science and Technology (JAMSTEC) and the University of Tokyo from January

Table 1. (continued)

PC04	PC04	PC04	PC04	PC04	PC04	PC04	PC04	PC04	PC04	PC04	PC04	PC04	PC04	PC04	PC04
5	5	5	6	6	6	6	7	7	7	7	8	8	8	8	8
32–34	52–54	82–84	2–4	32–34	52–54	82–84	2–4	32–34	52–54	82–84	2–4	32–34	52–54	62–64	72–74
3.80	3.99	4.29	4.50	4.80	5.00	5.30	5.50	5.80	6.00	6.30	6.50	6.80	7.00	7.10	7.20
49.4	48.5	50.0	49.9	50.1	49.7	50.0	50.2	49.6	48.2	49.7	50.2	49.3	49.5	49.5	49.7
0.85	0.85	0.86	0.86	0.80	0.80	0.83	0.89	0.80	0.77	0.76	0.79	0.79	0.75	0.73	0.70
16.5	16.5	16.6	16.9	16.4	16.7	16.4	16.6	16.4	16.4	16.4	16.6	15.9	16.4	16.0	16.1
8.48	8.33	8.55	8.66	8.12	8.20	8.09	8.57	8.08	7.95	7.74	8.13	7.90	7.73	7.58	7.29
1.26	1.27	1.22	1.33	1.17	1.38	1.28	1.36	1.87	1.72	1.57	1.77	1.76	1.64	1.65	1.53
2.82	2.80	2.75	2.87	2.67	2.57	2.53	2.68	2.68	2.63	2.50	2.50	2.37	2.27	2.25	2.16
1.76	2.14	1.70	1.79	1.60	1.64	1.71	1.80	1.69	2.12	1.72	1.96	2.04	2.38	2.21	2.38
4.41	5.37	4.56	4.22	4.74	4.88	4.59	4.14	4.43	5.32	4.73	4.01	4.55	5.16	4.79	4.74
3.23	3.63	3.33	3.37	3.56	3.72	3.63	3.59	3.64	3.93	3.75	3.79	3.81	3.97	3.86	3.95
0.53	0.54	0.49	0.53	0.46	0.51	0.54	0.55	0.60	0.62	0.58	0.67	0.75	0.83	0.83	0.98
10.8	10.0	9.97	9.59	10.4	9.90	10.4	9.63	10.3	10.3	10.6	9.52	10.8	9.36	10.6	10.4
100	100	100	100	100	100	100	100	100	100	100	100	100	100	100	100
64.4	66.8	55.3	67.4	56.1	71.2	66.5	73.7	78.3	83.4	68.4	79.6	81.3	92.7	88.5	105
100	97.9	91.9	100	90.3	105	97.6	102	123	125	116	115	127	117	118	118
18.4	18.0	15.8	17.7	15.8	18.7	19.2	19.8	22.4	22.1	19.6	21.5	24.0	26.0	26.5	31.9
77.3	75.5	66.8	74.4	65.9	78.5	80.8	83.4	94.3	92.2	81.3	90.0	101	110	111	136
18.3	17.3	15.4	17.1	15.3	17.8	18.7	19.1	21.1	21.0	18.9	20.5	23.7	25.5	26.3	31.8
4.58	4.38	3.92	4.35	3.85	4.45	4.67	4.72	5.33	5.10	4.53	5.04	5.83	6.36	6.51	7.93
20.5	19.9	17.9	19.6	17.4	20.2	21.1	21.4	24.1	23.4	21.1	23.3	26.3	28.7	29.8	36.0
3.20	3.04	2.77	2.97	2.69	3.03	3.21	3.26	3.66	3.57	3.19	3.48	4.00	4.32	4.50	5.44
20.5	19.1	17.3	19.0	16.9	19.3	20.5	20.3	23.3	22.4	20.1	21.8	24.9	26.9	28.3	33.8
4.24	3.99	3.66	4.00	3.55	4.00	4.21	4.21	4.81	4.61	4.15	4.48	5.17	5.53	5.79	6.97
12.3	11.6	10.6	11.6	10.3	11.8	12.3	12.1	13.8	13.2	11.9	12.9	14.7	15.8	16.6	19.8
1.75	1.64	1.49	1.64	1.44	1.64	1.69	1.68	1.95	1.86	1.64	1.80	2.02	2.18	2.27	2.69
11.0	10.4	9.48	10.5	9.14	10.4	10.8	10.8	12.1	11.8	10.3	11.5	12.7	13.9	14.2	16.9
1.73	1.60	1.48	1.64	1.42	1.64	1.73	1.69	1.91	1.87	1.62	1.79	1.97	2.13	2.19	2.60
119	121	100	124	97.2	122	117	125	131	140	115	136	142	162	163	198
477	472	414	476	407	489	480	503	561	571	497	549	597	638	644	753
283	280	249	281	247	296	287	302	344	348	308	332	363	377	378	431
194	193	165	195	160	194	193	201	216	223	189	217	234	261	266	322
0.66	0.65	0.71	0.67	0.69	0.66	0.62	0.61	0.67	0.67	0.72	0.64	0.66	0.54	0.56	0.46
26.5	26.5	24.6	28.1	24.0	25.8	25.3	26.7	25.9	26.3	23.2	25.6	25.2	26.0	24.6	26.9
157	144	149	145	146	143	151	142	159	153	138	140	140	129	135	131
36.7	39.9	31.5	37.6	31.7	35.3	31.9	34.7	43.8	37.1	31.0	30.8	29.0	28.0	25.2	26.1
139	133	125	137	120	147	145	144	176	171	156	159	195	161	171	158
201	211	162	181	132	210	160	197	414	254	216	248	262	217	216	238
300	313	314	361	318	331	317	373	447	370	360	373	361	336	336	340
144	140	134	148	126	139	127	141	143	139	129	133	135	122	125	123
81.4	81.2	76.8	86.2	81.7	91.7	83.9	85.0	89.5	88.5	79.5	83.1	80.2	78.1	77.9	80.8
191	188	184	205	176	190	184	195	187	192	175	194	196	197	199	205
144	137	136	143	132	139	141	142	153	147	150	144	147	128	133	132
10.9	10.9	10.1	11.1	10.3	11.8	11.2	11.4	12.2	11.8	11.6	11.0	11.2	9.69	9.82	9.99
63.6	64.7	66.4	74.0	64.5	67.6	64.8	64.1	75.6	71.8	70.0	69.0	72.8	63.4	67.5	62.4
287	267	272	276	255	283	277	268	285	278	268	273	293	274	281	280
3.65	3.20	3.48	3.25	3.36	3.22	3.53	3.23	3.79	3.46	3.82	3.40	3.71	3.14	3.35	3.35
0.67	0.62	0.64	0.64	0.65	0.66	0.68	0.67	0.74	0.66	0.75	0.62	0.66	0.55	0.58	0.58
41.0	75.3	39.2	40.4	37.3	41.2	39.2	40.2	47.5	47.1	44.1	44.5	48.0	41.4	43.1	41.3
9.40	9.22	9.05	8.87	8.26	8.82	8.80	9.04	11.1	10.9	10.9	10.2	11.0	10.6	10.7	11.6
2.34	2.26	2.24	2.36	2.13	2.26	2.23	2.29	2.44	2.36	2.10	2.23	2.33	2.29	2.27	2.39

Fe_2O_3: total iron as Fe_2O_3. Major element contents are normalized to 100 wt.% including LOI.*
The Ce anomaly (Ce/Ce) is defined quantitatively as $Ce/Ce^* = (2Ce/Ce_{PAAS})/(La/La_{PAAS} + Pr/Pr_{PAAS})$. Ce* is the hypothetical concentration that strictly trivalent Ce would have.*

Table 1. (continued)

Core	PC04	PC04	PC04	PC04	PC04	PC04	PC04	PC04	PC04	PC04	PC04	PC04	PC04	PC04	PC04
Section	8	8	9	9	9	9	9	9	9	9	9	9	9	10	10
Interval [cm]	82–84	92–94	2–4	12–14	22–24	32–34	42–44	52–54	62–64	72–74	82–84	92–94	102–104	2–4	12–14
Depth [mbsf]	7.30	7.40	7.49	7.59	7.69	7.79	7.89	7.99	8.09	8.19	8.29	8.39	8.49	8.57	8.67
SiO_2 (wt.%)	50.3	49.5	49.2	48.3	47.4	46.2	45.5	45.4	44.1	43.1	41.7	41.6	46.2	47.0	47.9
TiO_2	0.70	0.69	0.74	0.75	0.76	0.73	0.69	0.70	0.65	0.62	0.60	0.60	0.65	0.64	0.62
Al_2O_3	16.3	16.1	16.3	15.6	15.2	14.6	14.2	14.3	13.3	12.9	12.2	12.3	14.6	14.6	15.0
Fe_2O_3*	7.33	7.22	7.74	7.64	7.58	7.08	6.70	6.81	6.21	6.00	5.59	5.74	6.54	6.47	6.45
MnO	1.53	1.47	1.62	1.66	1.75	1.93	1.85	1.81	2.44	2.40	2.52	2.66	2.32	2.23	2.16
MgO	2.12	2.14	2.31	2.25	2.23	2.28	2.29	2.41	2.45	2.41	2.30	2.41	2.99	3.00	3.07
CaO	2.44	2.66	2.92	3.21	4.08	5.86	7.08	6.97	8.53	9.31	11.2	11.1	6.71	6.25	5.17
Na_2O	4.44	4.82	4.15	4.71	4.66	4.27	4.03	4.25	3.59	3.50	3.28	3.18	2.68	3.13	3.18
K_2O	3.91	3.91	3.87	3.72	3.62	3.36	3.36	3.52	3.35	3.37	3.26	3.34	3.87	3.79	3.88
P_2O_5	1.03	1.16	1.32	1.61	2.22	3.54	4.45	4.38	5.59	6.17	7.62	7.52	4.33	4.07	3.27
LOI	9.92	10.3	9.86	10.5	10.5	10.2	9.93	9.42	9.74	10.3	9.73	9.44	9.08	8.84	9.31
Total	100	100	100	100	100	100	100	100	100	100	100	100	100	100	100
La (ppm)	113	123	147	169	237	364	452	464	534	585	718	658	367	302	227
Ce	121	118	129	145	170	220	265	260	318	343	404	383	268	252	226
Pr	35.0	37.2	42.0	52.2	73.4	113	141	138	165	179	222	206	110	93.1	69.9
Nd	147	158	181	224	318	487	611	596	703	767	956	883	470	400	297
Sm	34.8	37.3	42.4	52.5	75.0	116	145	139	167	182	227	210	109	94.2	68.2
Eu	8.62	9.21	10.4	13.1	18.6	28.7	36.0	34.4	41.7	44.7	55.9	51.6	27.1	23.3	17.2
Gd	39.1	42.4	47.8	60.2	85.8	133	166	159	191	206	256	235	121	105	76.5
Tb	5.96	6.39	7.14	9.09	12.8	19.9	25.1	23.8	28.6	30.9	38.6	35.0	18.1	15.7	11.4
Dy	36.9	39.7	44.6	56.3	80.1	124	156	149	180	194	240	218	112	96.2	70.8
Ho	7.59	8.17	9.19	11.5	16.4	25.3	31.8	30.6	36.7	39.8	49.1	44.3	23.1	19.6	14.5
Er	21.7	23.5	26.0	32.8	46.3	71.7	90.1	86.1	104	113	139	125	65.1	55.1	40.6
Tm	2.97	3.17	3.53	4.43	6.24	9.62	12.1	11.6	14.1	15.2	18.7	16.7	8.77	7.40	5.51
Yb	18.4	19.8	22.1	27.6	38.2	58.3	73.2	71.1	85.9	92.3	113	101	53.7	44.8	33.2
Lu	2.84	3.02	3.40	4.20	5.82	8.91	11.1	10.9	13.0	14.0	17.1	15.2	8.12	6.80	5.11
Y	220	237	272	337	478	750	934	941	1126	1231	1515	1360	715	587	432
∑REY (ppm)	814	866	987	1200	1661	2529	3148	3114	3706	4036	4968	4542	2476	2104	1594
∑LREE	459	483	552	657	892	1328	1649	1631	1927	2100	2582	2392	1351	1165	905
∑HREE	355	384	436	543	769	1200	1498	1483	1779	1936	2386	2150	1125	938	690
Ce/Ce*	0.44	0.40	0.38	0.35	0.29	0.25	0.24	0.23	0.24	0.24	0.23	0.24	0.30	0.34	0.41
Sc (ppm)	29.0	28.7	27.6	34.1	41.1	52.4	63.6	61.0	72.9	78.7	90.6	83.9	59.1	52.7	46.8
V	136	130	135	149	150	134	129	126	122	118	114	116	121	123	124
Cr	27.7	24.2	27.5	30.0	30.3	32.3	32.8	32.4	30.3	27.3	28.2	27.3	31.4	32.6	34.3
Co	163	155	147	173	188	203	197	179	247	236	252	237	203	206	210
Ni	252	195	196	207	247	341	353	388	535	535	601	589	553	493	521
Cu	344	317	309	333	350	362	356	329	407	385	400	390	371	352	367
Zn	127	122	123	134	138	144	148	147	195	190	197	199	195	188	200
Rb	82.2	79.6	79.7	80.9	78.0	68.1	73.8	78.2	71.5	70.3	71.7	72.4	94.9	90.0	96.5
Sr	214	212	219	248	284	339	388	379	446	474	548	507	324	299	256
Zr	135	128	122	143	147	142	146	141	152	150	151	145	147	149	149
Nb	10.2	9.83	9.82	11.0	11.1	10.9	11.3	11.3	11.9	11.7	11.5	10.9	11.4	11.0	11.0
Mo	62.4	59.5	58.0	65.4	67.8	63.9	60.7	57.1	65.6	65.6	69.2	63.7	66.9	67.8	68.7
Ba	288	277	275	300	290	270	278	291	322	332	346	357	419	406	414
Hf	3.40	3.26	3.11	3.56	3.66	3.51	3.64	3.61	3.83	3.78	3.71	3.53	3.86	3.89	4.03
Ta	0.60	0.56	0.54	0.62	0.63	0.60	0.65	0.65	0.68	0.66	0.65	0.63	0.70	0.73	0.72
Pb	43.2	41.9	45.1	49.0	49.9	46.8	45.4	43.7	50.9	49.8	53.8	54.2	61.6	61.2	60.7
Th	12.4	12.2	13.5	14.8	17.5	22.9	27.7	27.5	29.5	30.8	36.4	33.5	18.2	16.5	11.6
U	2.52	2.52	2.75	3.09	3.60	4.60	5.47	5.46	6.29	6.74	7.97	7.45	4.90	4.62	3.77

21 to 31, 2013. Seven sediment cores were collected during the cruise from a deep-sea plain south and west off Takuyo Daigo seamount, in the southern part of the Minamitorishima EEZ. General descriptions of lithology and analytical results for all core samples are reported elsewhere (Fujinaga *et al.*, 2016). This paper focuses on piston cores PC04 and PC05, which contained anomalously REY-enriched stratigraphic layers. Photographs of the two sediment cores are given in Supplementary Fig. S1.

PC04 was collected at 21°56.11′ N, 152°39.51′ E (~60 km east of Ocean Drilling Program Site 800A where REY-rich mud was documented by Kato *et al.*, 2012), at a water depth of 5720 m (Fig. 1); 12.73 m of sediment core was recovered. The sediment is mainly composed of dark brown to brownish black clay (core top to 3.0 m below

Table 1. (continued)

PC04	PC04	PC04	PC04	PC04	PC04	PC04	PC04	PC04	PC04	PC04	PC04	PC04	PC04	PC04	PC04	PC04
10	10	10	10	10	11	11	11	11	12	12	12	12	13	13	13	13
22–24	32–34	42–44	82–84	92–94	32–34	42–44	82–84	92–94	32–34	42–44	82–84	92–94	32–34	42–44	82–84	90–92
8.77	8.87	8.97	9.37	9.47	9.87	9.97	10.37	10.47	10.87	10.97	11.37	11.47	11.86	11.96	12.36	12.44
47.5	48.3	47.8	49.0	48.6	48.5	47.8	47.7	47.3	47.8	47.2	47.5	46.7	47.9	46.4	48.7	48.6
0.59	0.60	0.60	0.59	0.60	0.60	0.60	0.57	0.58	0.56	0.57	0.54	0.55	0.53	0.51	0.52	0.55
15.0	15.3	15.5	15.4	15.5	14.9	15.0	14.7	14.9	14.8	14.9	14.5	14.4	14.1	14.0	14.3	14.6
6.30	6.46	6.45	6.30	6.32	6.18	6.14	5.92	5.97	5.70	5.81	5.52	5.49	5.44	5.22	5.45	5.68
2.11	2.10	2.07	1.84	1.84	2.19	2.13	2.22	2.33	2.22	2.24	1.90	2.01	1.93	1.84	1.66	1.62
3.07	3.09	3.16	3.10	3.11	3.12	3.13	3.10	3.15	2.98	3.04	2.88	2.90	2.87	2.73	2.79	2.90
5.21	4.98	4.75	4.63	5.06	4.93	5.27	5.70	6.05	5.83	5.85	6.36	7.03	6.17	7.31	5.74	5.85
3.19	3.06	3.59	3.16	2.69	3.25	3.52	3.37	2.73	3.15	3.41	3.27	2.84	3.27	3.87	3.12	3.47
3.82	3.84	4.00	3.94	4.06	3.92	4.20	3.78	4.00	4.04	4.05	4.01	4.17	4.02	4.36	4.20	4.35
3.32	3.15	2.92	2.92	3.19	3.09	3.24	3.65	3.85	3.74	3.71	4.15	4.57	3.96	4.65	3.66	3.70
9.89	9.17	9.17	9.09	9.04	9.26	9.03	9.35	9.13	9.20	9.17	9.33	9.31	9.79	9.15	9.86	8.61
100	100	100	100	100	100	100	100	100	100	100	100	100	100	100	100	100
223	190	209	194	241	225	275	270	315	260	282	294	325	255	283	192	223
227	206	225	200	207	198	218	217	235	208	210	207	210	201	194	180	193
69.5	58.6	61.3	59.1	69.2	66.4	77.2	79.9	90.5	73.3	74.0	83.1	88.1	73.2	73.1	53.4	59.2
294	248	260	251	296	280	327	339	386	313	317	352	374	308	310	224	250
69.0	57.2	59.9	58.6	67.8	64.5	74.3	78.2	88.1	71.7	70.9	80.0	83.5	70.6	69.3	51.2	56.3
17.1	14.4	14.7	14.5	16.7	16.0	18.2	19.4	21.7	17.9	17.5	19.7	20.5	17.3	17.1	12.6	13.9
76.0	63.4	64.7	64.1	74.5	71.8	82.3	87.2	98.4	81.5	80.6	91.4	94.6	79.7	79.8	58.1	63.4
11.3	9.39	9.60	9.53	11.1	10.7	12.3	13.1	14.7	12.2	12.1	13.6	14.2	11.8	12.0	8.78	9.52
69.7	58.5	59.0	59.2	68.6	66.7	75.9	81.9	91.1	77.9	76.7	86.4	89.4	74.5	77.2	56.0	60.4
14.0	11.8	12.0	12.0	14.0	13.7	15.5	16.7	18.7	16.3	16.1	18.0	18.7	15.3	16.3	11.8	12.7
39.4	32.8	33.7	33.5	39.3	38.5	43.9	47.0	52.4	46.8	46.6	51.2	53.5	43.4	47.4	34.3	36.8
5.33	4.45	4.56	4.51	5.28	5.19	5.94	6.37	7.11	6.47	6.45	7.04	7.37	5.96	6.64	4.81	5.12
32.0	26.7	27.8	27.3	32.2	31.8	36.5	38.8	43.7	40.7	40.6	43.3	46.2	36.2	41.7	30.4	32.5
4.91	4.07	4.22	4.10	4.77	4.83	5.43	5.82	6.54	6.27	6.14	6.57	6.93	5.50	6.34	4.62	4.99
418	350	377	355	436	408	489	500	586	504	521	553	608	469	536	364	410
1570	1336	1422	1346	1583	1500	1756	1800	2056	1736	1777	1906	2040	1667	1769	1286	1431
900	775	829	776	897	849	990	1003	1137	943	971	1036	1101	925	946	713	796
670	561	593	569	685	651	766	797	919	792	806	870	939	742	823	573	635
0.42	0.44	0.45	0.43	0.37	0.37	0.34	0.34	0.32	0.35	0.33	0.30	0.29	0.34	0.31	0.41	0.38
47.0	42.9	46.3	43.0	48.9	46.6	52.1	51.8	59.2	54.0	56.1	55.5	60.0	51.5	55.1	48.5	51.1
123	115	120	109	110	117	120	115	116	124	165	116	106	115	106	110	110
37.3	35.7	30.1	35.3	29.4	31.4	29.6	31.2	28.7	29.9	26.9	32.3	26.5	28.6	23.0	29.2	28.2
213	195	206	177	173	216	219	216	225	235	226	187	188	182	174	152	146
530	483	565	442	497	516	573	508	595	527	570	482	508	456	485	372	425
371	343	386	319	346	363	395	373	421	399	426	365	388	374	390	335	361
200	188	206	183	184	194	206	190	200	192	192	179	184	176	170	173	181
95.8	90.9	105	92.7	102	88.5	99.9	87.1	99.3	92.4	99.1	93.2	93.7	84.4	89.3	83.1	94.2
259	227	242	218	242	237	263	272	297	297	301	321	335	315	356	292	304
148	139	150	141	142	147	151	150	156	164	158	157	151	148	143	138	140
10.9	10.2	11.2	10.5	10.9	10.4	11.3	10.3	10.9	10.3	10.6	10.2	10.4	9.30	9.07	8.96	9.97
68.1	62.8	68.5	51.5	51.2	67.3	69.5	67.6	73.2	72.9	72.5	60.9	63.3	60.5	61.4	51.9	51.8
409	378	405	348	356	378	399	386	410	395	403	356	350	353	349	331	348
4.15	3.84	4.04	3.84	3.76	3.99	3.98	3.95	4.08	4.17	3.93	3.90	3.71	3.62	3.49	3.49	3.43
0.72	0.66	0.69	0.67	0.68	0.68	0.70	0.66	0.67	0.66	0.66	0.67	0.64	0.59	0.56	0.58	0.63
59.4	54.3	58.0	50.4	50.5	52.9	57.1	50.3	52.3	44.5	46.7	41.0	41.7	41.9	42.4	37.1	38.2
12.0	10.1	10.8	9.82	10.8	9.94	11.0	11.0	12.4	10.8	10.9	11.7	11.5	10.2	9.78	9.18	10.3
3.98	3.40	3.66	3.35	3.77	3.40	3.84	3.72	4.25	3.83	3.90	4.04	4.38	3.66	4.19	3.42	3.60

seafloor (mbsf) and 8.4 mbsf to the core bottom) and dark brown to brownish black clay with zeolite to zeolitic clay (3.0 to 7.7 mbsf) (Figs. 2a and S1a). Most zeolite minerals in the core are phillipsite. Major components of the sediments are clay-sized minerals, amorphous ferromanganese oxides, and euhedral phillipsite with characteristic rod-shaped or cruciform crystal morphology as described by Marsaglia *et al*. (2013). The interval of 7.7 to 8.4 mbsf is characterized by abundant silt-sized grains of phillipsite and phosphate. The phosphate grains are characterized by low birefringence and typical interference colors of first-order dark to pale gray under a polarizing microscope. The grains are very irregularly shaped and have complex textures that are completely different from igneous or authigenic crystalline apatite (Ohta *et al*., 2016). This suggests that they are of biogenic origin

Table 2. Major, trace, and rare-earth element data of KR13-02 PC05

Core	PC05	PC05	PC05	PC05	PC05	PC05	PC05	PC05	PC05	PC05	PC05	PC05	PC05	PC05
Section	1	1	1	2	2	3	3	3	3	3	3	3	3	3
Interval [cm]	2–4	12–14	22–24	32–34	82–84	2–4	12–14	22–24	32–34	40–42	52–54	62–64	72–74	82–84
Depth [mbsf]	0.03	0.13	0.23	0.595	1.095	1.3	1.4	1.5	1.6	1.68	1.8	1.9	2	2.1
SiO_2 (wt.%)	52.1	53.0	52.4	49.2	48.7	47.9	47.4	47.8	47.8	47.9	47.7	47.6	48.0	46.8
TiO_2	0.86	0.86	0.86	0.84	0.71	0.78	0.74	0.82	0.78	0.79	0.81	0.79	0.80	0.74
Al_2O_3	16.8	16.6	16.5	16.1	16.0	15.6	15.3	15.9	15.5	15.5	15.4	15.3	15.8	15.1
Fe_2O_3*	8.41	8.43	8.43	8.18	6.90	7.78	7.47	8.08	7.73	7.78	7.84	7.72	7.96	7.34
MnO	0.81	0.81	0.96	1.36	1.35	1.70	1.84	1.84	1.80	1.78	1.75	1.74	1.68	1.83
MgO	3.32	3.27	3.26	2.72	2.48	2.53	2.34	2.61	2.54	2.55	2.48	2.45	2.49	2.29
CaO	1.78	1.38	1.41	1.86	1.74	2.27	2.81	2.38	2.19	2.26	2.34	2.45	2.85	2.65
Na_2O	3.74	3.28	3.28	4.47	5.43	4.75	4.77	5.37	4.85	4.80	4.79	4.86	5.46	4.74
K_2O	3.49	3.40	3.39	3.66	3.73	3.66	3.81	3.92	3.71	3.68	3.74	3.78	3.79	3.70
P_2O_5	0.28	0.27	0.31	0.71	0.62	0.93	1.27	0.88	0.87	0.91	0.95	1.03	1.12	1.17
LOI	8.41	8.73	9.15	10.9	12.4	12.1	12.2	10.4	12.2	12.1	12.2	12.3	10.1	13.6
Total	100	100	100	100	100	100	100	100	100	100	100	100	100	100
La (ppm)	55.5	45.2	50.8	76.4	61.3	85.3	123	96.5	80.1	87.1	87.9	95.0	130	111
Ce	111	101	105	99.1	109	117	125	141	125	129	121	121	145	122
Pr	14.6	12.4	14.3	21.6	17.9	24.4	37.4	26.2	23.6	25.9	25.9	27.8	36.8	33.4
Nd	55.6	48.5	56.6	91.3	73.6	103	161	106	99.3	108	109	119	150	143
Sm	12.6	10.6	12.9	21.0	17.1	24.0	38.1	25.1	23.2	25.7	25.3	27.9	36.2	33.6
Eu	2.92	2.54	2.96	5.15	4.00	5.93	9.38	6.23	5.78	6.30	6.32	6.82	8.82	8.33
Gd	12.9	10.9	13.4	24.2	19.1	27.7	43.5	28.1	26.2	28.9	29.3	31.7	40.7	38.8
Tb	1.96	1.63	2.03	3.64	2.94	4.09	6.50	4.26	3.93	4.28	4.38	4.72	6.11	5.82
Dy	12.3	10.3	12.6	23.0	18.2	25.8	40.3	26.7	24.6	26.6	27.0	29.7	37.8	35.9
Ho	2.43	2.05	2.56	4.81	3.71	5.35	8.23	5.40	5.03	5.51	5.54	6.10	7.73	7.36
Er	7.11	6.03	7.46	13.8	10.6	15.3	23.4	15.6	14.5	15.7	15.9	17.5	22.0	20.8
Tm	1.03	0.88	1.07	1.96	1.46	2.13	3.18	2.19	2.00	2.15	2.19	2.41	3.02	2.87
Yb	6.86	5.65	6.85	12.5	9.21	13.4	19.7	14.0	12.5	13.6	13.8	15.0	19.0	17.7
Lu	1.05	0.88	1.08	1.96	1.41	2.06	3.01	2.16	1.97	2.09	2.12	2.29	2.91	2.74
Y	65.5	54.4	68.8	135	104	151	237	160	142	154	158	173	231	213
∑REY (ppm)	363	312	358	536	453	608	878	659	590	635	633	679	877	796
∑LREE	252	220	242	314	283	360	493	401	357	382	375	397	506	451
∑HREE	111	92.7	116	221	170	247	384	258	233	253	258	282	370	345
Ce/Ce*	0.89	0.97	0.89	0.56	0.75	0.59	0.42	0.64	0.66	0.62	0.58	0.54	0.48	0.46
Sc (ppm)	25.0	19.6	21.5	23.8	19.9	24.5	28.2	29.4	24.8	24.5	24.1	24.4	32.6	26.9
V	184	164	168	140	113	136	134	142	139	142	134	133	142	131
Cr	97.9	83.4	76.3	34.0	31.5	30.4	31.6	32.3	33.2	32.0	28.7	32.2	31.6	29.5
Co	95.0	77.1	94.8	137	127	168	184	219	186	190	189	185	235	188
Ni	179	136	193	375	167	258	310	382	261	282	266	254	366	280
Cu	274	219	260	328	306	342	355	414	334	350	332	333	428	342
Zn	169	134	145	157	124	145	132	187	139	143	134	135	173	131
Rb	145	123	126	78.6	67.6	71.5	68.9	91.9	72.6	75.2	69.4	67.7	87.6	68.6
Sr	194	168	180	170	154	197	221	225	200	207	200	204	242	213
Zr	155	127	138	145	144	146	130	169	144	149	142	137	166	129
Nb	15.5	14.3	15.4	11.2	11.5	11.0	9.81	12.6	11.1	11.4	10.6	10.2	12.0	9.83
Mo	13.8	15.7	16.5	36.6	69.6	86.5	83.5	101	89.3	90.0	86.0	83.5	93.3	83.5
Ba	658	515	514	289	227	259	264	357	271	279	267	257	344	259
Hf	3.52	3.15	3.46	3.40	3.79	3.61	3.26	4.03	3.60	3.72	3.50	3.35	3.82	3.16
Ta	1.03	1.02	1.06	0.71	0.83	0.66	0.57	0.65	0.64	0.66	0.62	0.58	0.59	0.56
Pb	41.4	39.2	42.7	38.4	39.5	44.1	43.5	50.5	45.6	47.0	44.6	43.4	47.1	43.1
Th	14.7	13.4	13.9	9.81	11.8	10.0	11.5	11.3	10.4	11.1	10.3	10.3	11.9	10.7
U	2.71	2.39	2.52	2.22	1.88	2.47	2.58	2.84	2.47	2.54	2.44	2.47	2.89	2.49

(e.g., fish teeth or bone debris as described by Marsaglia *et al*., 2015). Therefore, we hereafter describe the phosphate as biogenic calcium phosphate (BCP). Scattered ferromanganese micronodules (<1 mm) are highly abundant at depths from 1.7 to 2.1 and 2.7 to 3.4 mbsf, and moderately abundant at depths from 0.6 to 1.0, 5.0 to 5.3, and 7.4 to 8.5 mbsf. The sediment is homogeneous except for the intervals 2.7 to 4.1, 4.9 to 5.2, and 6.5 to 7.5,

Table 2. (continued)

PC05	PC05	PC05	PC05	PC05	PC05	PC05	PC05	PC05	PC05	PC05	PC05	PC05	PC05	PC05
4	4	4	4	4	4	4	4	4	4	5	5	5	5	5
2–4	12–14	22–24	32–34	42–44	52–54	62–64	72–74	82–84	92–94	2–4	12–14	22–24	32–34	42–44
2.27	2.37	2.47	2.57	2.67	2.77	2.87	2.97	3.07	3.17	3.27	3.37	3.47	3.57	3.67
46.3	46.8	46.0	44.9	44.3	42.5	42.1	38.9	37.3	38.6	38.5	40.0	41.3	45.2	47.3
0.75	0.74	0.79	0.85	0.82	0.77	0.71	0.62	0.58	0.58	0.57	0.56	0.57	0.60	0.62
14.9	15.1	15.3	14.3	13.9	13.2	12.9	11.7	10.9	11.5	11.5	11.9	12.8	14.3	15.4
7.49	7.50	7.92	7.87	7.66	7.09	6.48	5.58	5.11	5.33	5.38	5.68	6.05	6.67	6.87
1.87	1.86	2.06	2.33	2.42	2.58	2.15	1.64	1.46	1.51	1.51	1.72	1.96	2.04	1.94
2.32	2.31	2.44	2.36	2.43	2.39	2.30	2.17	2.03	2.07	2.06	2.15	2.36	2.75	3.01
3.16	3.56	4.59	5.90	7.14	8.73	10.1	14.6	16.2	14.9	14.8	13.1	10.8	7.13	4.96
4.81	4.75	5.07	4.48	4.35	3.93	3.80	2.87	3.30	3.39	3.52	3.98	4.22	3.63	3.59
3.50	3.60	3.51	3.31	3.19	3.18	3.12	3.01	2.86	3.17	3.24	2.85	3.44	3.64	3.89
1.55	1.87	2.29	3.57	4.47	5.66	6.75	10.0	11.2	10.3	10.0	8.89	7.17	4.68	3.18
13.3	12.0	10.0	10.2	9.35	9.94	9.61	8.80	9.00	8.67	8.92	9.19	9.33	9.27	9.27
100	100	100	100	100	100	100	100	100	100	100	100	100	100	100
140	173	225	337	423	553	642	1252	981	878	903	778	607	459	275
129	137	149	194	230	280	309	424	437	394	400	345	273	271	220
42.9	52.4	70.9	105	133	174	201	289	304	272	281	242	182	138	87.5
184	227	296	457	576	754	870	1225	1317	1178	1213	1042	760	588	377
43.4	53.8	71.9	109	137	180	206	293	313	280	290	248	185	143	91.6
10.8	13.2	17.8	27.1	33.9	44.2	50.9	72.9	77.0	69.2	71.5	61.3	45.9	34.9	22.2
49.6	61.2	82.1	125	156	201	235	334	354	317	325	279	211	157	101
7.48	9.12	12.2	18.6	23.1	30.1	34.8	49.8	52.5	47.0	48.1	41.1	31.0	23.1	14.9
46.1	56.7	75.8	115	144	188	217	310	328	293	299	255	191	141	90.2
9.54	11.6	15.6	23.6	29.2	38.0	44.2	63.7	67.1	59.6	61.0	51.8	38.7	28.7	18.2
26.7	33.1	43.6	65.9	81.9	106	123	179	188	167	170	144	108	79.9	50.3
3.64	4.49	5.93	8.89	11.1	14.3	16.5	24.0	25.3	22.4	22.8	19.1	14.4	10.6	6.75
22.5	27.5	36.6	54.2	66.7	85.6	99.9	146	153	135	137	115	86.5	63.2	40.6
3.40	4.21	5.56	8.27	10.1	13.2	15.1	22.0	23.0	20.3	20.6	17.2	12.8	9.54	6.09
273	343	444	683	877	1154	1338	2114	2057	1823	1864	1580	1190	908	533
993	1206	1553	2331	2932	3815	4402	6799	6677	5955	6106	5220	3937	3055	1934
551	655	831	1229	1533	1985	2278	3556	3430	3071	3158	2717	2053	1634	1073
442	551	722	1103	1399	1831	2124	3243	3247	2885	2948	2503	1883	1421	861
0.38	0.33	0.27	0.23	0.22	0.21	0.20	0.16	0.18	0.18	0.18	0.18	0.19	0.25	0.32
29.1	31.3	38.0	47.0	58.3	72.3	81.5	106	116	105	110	95.9	67.2	63.8	45.9
130	130	161	138	140	134	116	90.9	83.7	86.8	94.5	93.4	102	135	132
28.9	27.9	32.3	29.8	33.3	35.9	34.3	29.6	29.8	26.7	28.0	27.7	30.6	38.9	43.0
186	189	217	226	257	282	220	152	142	140	144	145	152	196	182
349	276	316	355	417	496	406	362	327	284	297	285	372	450	368
363	328	368	366	397	405	360	310	286	274	278	270	270	311	281
134	129	150	143	171	180	165	155	162	151	160	149	136	164	160
65.5	67.0	71.7	58.8	62.9	64.7	62.3	57.1	55.0	56.2	59.8	60.3	61.4	106	112
220	240	262	317	380	453	487	559	673	618	642	572	398	396	282
127	133	144	150	157	159	156	32.7	126	143	152	143	122	166	154
9.70	10.2	11.1	12.0	12.5	13.1	13.1	8.66	10.2	10.3	10.8	10.3	8.93	12.0	11.4
78.2	78.3	87.1	85.8	89.1	86.2	70.8	50.2	48.9	50.1	56.3	61.4	67.5	89.4	82.4
255	257	284	249	256	266	241	223	216	227	243	249	253	359	356
3.12	3.18	3.59	3.60	3.79	3.89	3.78	1.29	2.79	3.41	3.62	3.46	3.62	4.06	3.90
0.55	0.58	0.67	0.66	0.66	0.67	0.74	0.38	0.21	0.49	0.63	0.57	0.57	0.71	0.73
43.3	45.6	50.9	50.3	51.8	51.1	41.8	35.5	32.0	32.8	36.2	37.9	40.4	54.3	54.5
11.9	13.6	16.2	19.6	22.8	27.5	30.8	40.1	42.4	39.1	40.4	35.8	31.7	28.9	23.8
2.69	3.00	3.64	4.39	4.88	5.82	6.48	9.52	10.3	9.62	10.2	9.04	7.71	6.25	4.74

Fe_2O_3: total iron as Fe_2O_3. Major element contents are normalized to 100 wt.% including LOI.*
The Ce anomaly (Ce/Ce) is defined quantitatively as $Ce/Ce^* = (2Ce/Ce_{PAAS})/(La/La_{PAAS} + Pr/Pr_{PAAS})$. Ce* is the hypothetical concentration that strictly trivalent Ce would have.*

Table 2. (continued)

Core	PC05	PC05	PC05	PC05	PC05	PC05	PC05	PC05	PC05	PC05	PC05	PC05	PC05	PC05
Section	5	5	5	5	5	6	6	6	6	6	6	6	6	6
Interval [cm]	52–54	62–64	72–74	82–84	92–94	2–4	12–14	22–24	32–34	42–44	52–54	62–64	72–74	82–84
Depth [mbsf]	3.77	3.87	3.97	4.07	4.17	4.27	4.37	4.47	4.57	4.67	4.77	4.87	4.97	5.07
SiO_2 (wt.%)	48.4	48.9	48.6	49.3	49.7	48.0	49.8	48.8	49.8	50.0	49.3	49.7	49.1	49.7
TiO_2	0.63	0.63	0.63	0.63	0.63	0.62	0.63	0.62	0.64	0.63	0.63	0.63	0.63	0.63
Al_2O_3	16.0	16.2	16.7	16.4	16.4	15.6	16.5	16.9	16.4	16.4	16.2	16.3	16.7	16.2
Fe_2O_3*	7.05	7.12	7.17	7.23	7.18	6.95	7.29	7.21	7.28	7.26	7.16	7.23	7.22	7.19
MnO	1.88	1.82	1.71	1.87	1.83	1.92	1.92	1.88	2.03	1.97	2.03	2.06	2.04	2.04
MgO	3.11	3.17	3.19	3.20	3.20	3.02	3.19	3.16	3.18	3.16	3.12	3.15	3.13	3.14
CaO	3.89	3.39	2.94	2.72	2.52	4.50	2.41	2.35	2.35	2.50	2.81	2.46	2.40	2.48
Na_2O	3.38	3.43	3.86	3.58	3.62	3.44	3.59	3.87	3.56	3.54	3.56	3.56	3.66	3.62
K_2O	4.02	4.03	4.30	4.09	4.05	3.88	4.02	4.26	4.05	4.05	4.02	4.03	4.01	4.02
P_2O_5	2.40	2.07	1.53	1.57	1.43	2.84	1.35	1.20	1.30	1.40	1.62	1.38	1.31	1.38
LOI	9.28	9.29	9.34	9.36	9.39	9.24	9.29	9.74	9.36	9.07	9.55	9.44	9.85	9.56
Total	100	100	100	100	100	100	100	100	100	100	100	100	100	100
La (ppm)	214	187	156	140	130	244	128	126	130	144	158	136	144	139
Ce	210	206	187	180	168	222	177	175	184	192	192	184	185	185
Pr	68.2	60.4	46.1	44.4	41.3	77.4	40.4	37.6	41.2	45.7	50.1	43.1	43.0	44.5
Nd	291	256	189	187	175	330	169	155	171	192	211	180	175	186
Sm	70.6	61.8	45.9	44.7	42.0	79.5	40.9	37.3	41.4	46.3	51.0	43.1	42.3	45.2
Eu	17.3	15.2	11.2	11.0	10.1	19.4	9.90	9.06	9.95	11.2	12.4	10.6	10.4	10.9
Gd	77.4	67.3	49.4	48.8	45.3	86.7	43.6	39.3	43.9	49.0	54.8	46.5	45.9	48.1
Tb	11.5	10.0	7.35	7.22	6.71	12.9	6.50	5.92	6.58	7.34	8.19	6.98	6.82	7.20
Dy	69.8	61.1	45.0	44.2	40.7	79.2	39.6	35.8	40.1	44.8	49.7	42.2	41.4	43.6
Ho	14.0	12.3	8.92	8.90	8.19	15.9	7.93	7.21	7.93	8.89	9.97	8.46	8.22	8.68
Er	39.0	34.1	25.1	24.8	22.6	44.3	22.0	20.1	22.3	24.8	27.7	23.5	22.8	24.0
Tm	5.26	4.59	3.38	3.38	3.04	5.96	2.95	2.72	3.02	3.34	3.75	3.20	3.10	3.25
Yb	31.7	27.9	20.9	20.5	18.5	36.1	18.0	16.6	18.4	20.4	22.9	19.3	19.1	19.9
Lu	4.77	4.22	3.08	3.07	2.78	5.46	2.69	2.48	2.73	3.05	3.44	2.89	2.82	2.95
Y	409	356	260	256	236	459	228	214	231	259	288	241	235	250
∑REY (ppm)	1533	1364	1057	1024	950	1718	936	883	955	1051	1143	991	984	1019
∑LREE	871	787	634	607	567	973	565	539	578	631	675	597	599	611
∑HREE	662	577	423	417	383	746	371	344	376	420	468	394	385	408
Ce/Ce*	0.40	0.44	0.50	0.52	0.52	0.37	0.56	0.58	0.57	0.54	0.49	0.55	0.54	0.53
Sc (ppm)	40.2	38.4	31.1	31.1	29.4	41.6	29.6	31.5	30.4	33.6	33.7	31.3	32.8	33.1
V	139	146	133	135	130	128	135	135	142	145	139	138	136	138
Cr	42.8	42.0	40.6	39.3	36.7	38.5	39.0	40.6	44.5	41.3	38.6	41.5	37.9	39.3
Co	185	186	187	175	166	176	166	182	182	185	181	181	193	178
Ni	371	369	431	418	348	377	379	400	377	417	442	373	453	382
Cu	275	269	276	252	243	250	239	252	244	251	249	239	264	241
Zn	167	170	184	164	161	165	160	173	167	173	171	165	189	166
Rb	124	133	132	123	119	113	121	126	124	129	122	118	125	122
Sr	243	231	186	189	182	258	184	157	189	207	211	196	192	199
Zr	155	159	147	143	142	146	144	132	151	155	149	148	143	151
Nb	11.8	12.1	11.9	11.3	11.3	11.6	11.5	11.0	12.1	12.3	11.7	11.5	11.8	11.8
Mo	80.8	81.0	74.6	74.7	73.7	74.6	75.4	75.0	80.1	82.6	79.7	80.4	78.5	77.7
Ba	378	397	432	356	359	355	376	377	396	406	387	387	442	394
Hf	4.06	4.02	3.76	3.76	3.67	3.75	3.74	3.34	3.93	4.06	3.91	3.91	3.69	3.92
Ta	0.78	0.80	0.73	0.75	0.73	0.75	0.74	0.74	0.78	0.79	0.77	0.76	0.75	0.77
Pb	56.0	57.4	53.5	52.3	51.7	52.6	53.2	55.3	59.2	60.1	58.4	58.6	57.4	58.9
Th	22.5	22.1	19.2	18.0	16.5	21.3	16.9	16.0	17.0	18.2	18.4	17.4	17.2	17.5
U	4.14	3.91	3.33	3.08	2.82	4.03	2.77	2.64	2.81	3.04	3.14	2.83	2.80	2.80

and 10.6 mbsf to the core bottom, which are slightly bioturbated. Lighter brownish black colored patches are mottled by darker brownish black colored burrows between 10.6 mbsf and the core bottom.

PC05 was collected at 21°59.03′ N, 153°56.35′ E, ~260 km south of Minamitorishima Island, at a water depth of 5735 m (Fig. 1); 11.45 m of sediment core was recovered. The sediment is composed of dark brown to

Table 2. (continued)

PC05	PC05	PC05	PC05	PC05	PC05	PC05	PC05	PC05	PC05	PC05	PC05	PC05	PC05	PC05
6	7	7	7	7	7	7	7	7	7	7	8	8	8	8
92–94	2–4	12–14	22–24	32–34	42–44	52–54	62–64	72–74	82–84	92–94	2–4	12–14	22–24	32–34
5.17	5.27	5.37	5.47	5.57	5.67	5.77	5.87	5.97	6.07	6.17	6.27	6.37	6.47	6.57
49.6	49.8	50.0	49.3	50.1	49.9	50.4	50.4	49.5	51.0	50.7	50.6	50.3	48.6	49.0
0.63	0.63	0.61	0.61	0.61	0.62	0.61	0.61	0.60	0.60	0.61	0.60	0.60	0.60	0.60
16.1	16.4	16.6	16.8	16.5	16.5	16.7	16.7	16.7	16.9	16.8	16.6	16.6	16.4	16.0
7.25	7.32	7.42	7.25	7.30	7.33	7.38	7.29	7.11	7.22	7.19	7.00	7.12	6.94	6.75
2.02	2.03	2.16	2.04	2.04	2.03	2.06	1.99	1.90	1.91	1.95	2.03	1.93	2.25	2.44
3.10	3.15	3.18	3.14	3.16	3.13	3.15	3.17	3.11	3.12	3.09	3.08	3.07	3.07	3.04
2.81	2.36	1.98	2.25	2.13	2.34	1.90	1.98	2.05	1.90	2.16	2.41	2.53	2.93	3.78
3.58	3.60	3.59	3.75	3.55	3.60	3.60	3.64	4.05	3.53	3.54	3.55	3.53	3.95	3.48
4.02	4.07	3.97	4.18	4.08	4.01	4.13	4.25	4.57	4.15	4.09	4.02	4.07	4.22	3.88
1.62	1.29	1.03	1.08	1.13	1.28	0.95	0.97	0.93	0.95	1.14	1.32	1.38	1.64	2.28
9.29	9.37	9.50	9.63	9.32	9.26	9.03	9.05	9.50	8.75	8.81	8.80	8.94	9.42	8.76
100	100	100	100	100	100	100	100	100	100	100	100	100	100	100
153	131	105	118	113	129	96.6	98.9	77.3	107	127	147	161	162	232
187	182	169	179	171	183	166	165	115	169	177	187	197	166	221
49.7	41.9	33.5	36.0	35.5	40.6	29.6	30.3	23.5	33.0	40.2	47.8	52.7	54.5	75.5
207	175	139	148	149	170	123	126	95.6	139	170	202	224	224	323
49.9	42.5	33.6	35.8	36.2	41.0	30.0	30.7	23.2	33.4	41.0	49.1	54.5	55.2	78.6
12.3	10.2	8.08	8.69	8.72	9.92	7.15	7.37	5.74	8.01	10.0	12.1	13.3	13.6	19.5
54.6	45.1	35.5	37.9	38.0	43.7	31.4	32.4	25.5	35.2	43.3	52.3	57.5	60.0	85.3
8.08	6.73	5.32	5.60	5.74	6.53	4.69	4.85	3.84	5.27	6.55	7.82	8.72	8.86	12.9
49.1	40.7	32.2	34.4	34.7	39.9	28.8	29.5	23.6	32.5	40.1	47.2	52.7	54.0	77.7
9.81	8.11	6.42	6.82	6.90	8.03	5.83	5.98	4.79	6.57	8.06	9.45	10.5	10.6	15.5
27.1	22.6	17.9	19.0	19.5	22.7	16.5	17.0	13.6	18.6	22.7	26.0	28.9	29.3	42.7
3.68	3.05	2.41	2.58	2.63	3.06	2.25	2.30	1.87	2.52	3.04	3.50	3.92	3.89	5.70
22.5	18.6	14.8	15.8	16.0	18.9	13.8	14.3	11.7	15.3	18.4	21.0	23.2	23.6	33.7
3.34	2.77	2.20	2.33	2.38	2.84	2.09	2.15	1.74	2.31	2.73	3.12	3.44	3.44	4.89
280	233	182	197	196	230	166	172	129	187	227	267	294	284	440
1118	963	788	846	835	950	724	739	557	795	936	1082	1186	1152	1668
660	582	489	525	513	574	452	459	341	490	565	645	703	675	950
458	381	299	321	322	376	272	280	216	305	372	437	483	478	718
0.49	0.56	0.65	0.63	0.61	0.58	0.71	0.69	0.62	0.65	0.56	0.51	0.49	0.40	0.38
33.1	31.0	27.1	30.3	27.5	29.9	26.6	26.1	15.5	28.2	31.0	32.5	35.7	31.5	41.2
134	138	136	138	133	141	135	135	131	140	140	138	147	127	133
38.1	40.6	42.6	40.6	43.5	44.8	47.6	50.2	57.8	44.4	42.5	42.0	39.3	36.0	37.7
170	177	175	191	176	188	178	174	156	174	177	179	194	190	222
358	370	384	431	382	389	372	365	382	392	404	443	437	444	543
229	231	231	253	230	245	236	236	228	248	256	268	267	264	306
158	164	162	182	162	167	162	164	164	174	175	176	171	168	182
115	123	121	127	121	126	123	122	109	133	128	127	130	104	111
207	193	177	162	187	214	187	210	146	207	203	210	218	177	249
143	149	141	137	145	155	149	153	122	159	156	156	163	125	148
11.3	11.5	10.9	11.1	11.1	11.7	11.2	11.2	9.85	12.0	12.0	12.1	12.5	10.3	11.7
72.6	74.3	74.3	74.7	73.0	74.8	72.4	70.1	62.2	70.4	70.0	70.4	79.5	63.6	75.0
372	390	382	404	398	413	412	435	417	431	420	414	434	364	402
3.78	3.85	3.73	3.45	3.80	4.14	3.95	4.19	3.41	4.25	4.15	4.18	4.31	3.44	3.92
0.75	0.74	0.72	0.73	0.74	0.77	0.73	0.75	0.73	0.81	0.81	0.81	0.85	0.71	0.75
57.1	58.5	59.6	62.6	58.9	60.5	57.7	58.3	55.9	61.0	61.4	60.6	61.8	54.3	61.7
17.9	17.0	15.4	15.7	15.8	16.3	14.3	14.6	11.8	15.5	16.4	17.5	18.4	16.4	19.0
2.95	2.73	2.45	2.53	2.52	2.79	2.35	2.38	2.23	2.54	2.65	2.77	2.97	2.70	3.39

brownish black clay (core top to 1.7 and 3.7 to 7.4 mbsf) and dark brown to brownish black clay with zeolite to zeolitic clay (1.7 to 3.7 mbsf and 7.4 mbsf to the core bottom) (Figs. 2b and S1b). As with PC04, the major components of the sediments are clay minerals, amorphous ferromanganese oxides, and euhedral phillipsite (Fig. 2b). The depths from 2.5 to 3.6 mbsf and 6.5 to 7.2 mbsf contain abundant silt-sized grains of phillipsite and BCP (Fig.

Table 2. (continued)

Core	PC05	PC05	PC05	PC05	PC05	PC05	PC05	PC05	PC05	PC05	PC05	PC05	PC05
Section	8	8	8	8	8	8	9	9	9	9	9	9	9
Interval [cm]	42–44	52–54	62–64	72–74	82–84	92–94	2–4	12–14	22–24	32–34	42–44	52–54	62–64
Depth [mbsf]	6.67	6.77	6.87	6.97	7.07	7.17	7.26	7.36	7.46	7.56	7.66	7.76	7.86
SiO_2 (wt.%)	47.8	46.6	44.8	45.1	47.0	47.5	48.3	48.8	47.7	48.2	49.3	50.5	50.7
TiO_2	0.63	0.58	0.55	0.64	0.61	0.55	0.55	0.55	0.53	0.49	0.52	0.54	0.53
Al_2O_3	15.3	14.5	13.5	13.8	14.0	14.2	14.3	14.2	14.0	13.9	13.9	14.2	14.2
Fe_2O_3*	6.67	5.97	5.28	5.62	5.61	5.43	5.43	5.38	5.22	5.00	5.28	5.53	5.33
MnO	2.44	2.12	1.89	1.76	1.72	1.83	1.79	1.74	1.86	2.15	1.96	1.76	1.78
MgO	2.99	2.86	2.73	2.90	2.92	2.92	2.96	2.97	2.93	3.50	3.07	2.98	2.88
CaO	5.11	6.89	9.30	7.96	7.55	7.18	6.72	6.49	6.19	6.53	6.20	5.31	5.36
Na_2O	3.29	3.28	3.23	3.70	3.25	3.23	3.18	3.28	3.84	3.56	3.30	3.34	3.37
K_2O	3.87	3.88	3.89	4.16	3.94	4.15	4.12	4.14	4.48	3.63	4.04	4.16	4.27
P_2O_5	3.21	4.50	6.18	5.24	4.97	4.67	4.37	4.21	3.94	4.03	3.99	3.35	3.39
LOI	8.70	8.84	8.60	9.14	8.37	8.27	8.29	8.27	9.36	8.99	8.37	8.32	8.13
Total	100	100	100	100	100	100	100	100	100	100	100	100	100
La (ppm)	297	361	452	329	332	304	267	260	215	224	236	230	224
Ce	232	244	254	174	208	207	195	192	155	201	200	193	190
Pr	97.1	113	134	92.0	96.3	87.4	76.9	74.7	63.6	64.0	66.0	68.5	65.4
Nd	418	484	571	376	405	368	323	313	260	266	280	286	274
Sm	101	116	133	88.8	93.4	84.1	74.9	72.2	61.0	61.4	64.5	66.4	63.4
Eu	25.3	29.0	33.0	22.1	23.0	20.9	18.4	17.8	15.0	15.2	15.7	16.2	15.7
Gd	111	129	151	102	106	95.3	84.0	81.5	68.7	69.2	72.3	73.4	70.6
Tb	16.7	19.4	22.8	15.2	15.8	14.3	12.6	12.2	10.2	10.4	10.9	11.0	10.6
Dy	101	120	142	95.4	99.6	90.7	79.9	76.8	64.0	66.2	69.2	68.3	66.6
Ho	20.0	24.3	29.6	20.1	20.7	19.0	16.8	16.0	13.2	13.9	14.5	13.9	13.8
Er	54.2	67.4	84.2	57.5	59.0	54.0	48.1	45.6	37.5	40.4	41.9	38.9	39.1
Tm	7.16	9.09	11.6	7.97	8.12	7.53	6.68	6.27	5.19	5.71	5.84	5.30	5.35
Yb	42.3	54.6	71.1	50.0	49.9	46.9	41.5	38.8	32.3	36.1	36.4	32.2	32.8
Lu	6.15	8.12	10.7	7.54	7.64	7.11	6.32	5.85	4.82	5.52	5.59	4.79	4.90
Y	564	705	902	588	633	577	515	487	378	433	441	416	416
∑REY (ppm)	2092	2485	3001	2026	2156	1983	1766	1700	1384	1511	1560	1525	1493
∑LREE	1170	1348	1576	1083	1157	1071	955	930	770	831	862	861	832
∑HREE	922	1137	1425	944	999	912	811	770	614	680	698	664	660
Ce/Ce*	0.31	0.27	0.24	0.23	0.27	0.29	0.31	0.32	0.30	0.38	0.37	0.35	0.36
Sc (ppm)	45.8	57.8	73.6	51.6	58.5	56.9	52.8	50.7	40.2	51.4	45.8	47.1	46.1
V	121	116	105	102	107	108	104	97.1	97.0	89.2	97.3	101	101
Cr	35.5	32.3	29.6	32.0	31.2	26.9	27.1	25.4	25.3	20.0	25.4	26.3	24.3
Co	190	192	190	154	172	182	173	163	155	205	176	166	168
Ni	539	520	492	476	482	502	520	424	401	330	397	412	449
Cu	303	322	350	321	359	376	375	354	327	509	424	368	375
Zn	172	172	169	165	175	177	176	182	167	292	210	176	165
Rb	99.5	93.0	85.5	70.5	86.0	92.1	89.8	87.1	72.6	77.9	85.4	88.6	86.0
Sr	274	329	406	277	340	335	311	297	226	285	285	274	285
Zr	143	150	154	133	167	165	159	154	124	146	147	150	148
Nb	11.2	11.1	10.9	10.8	12.5	10.8	10.4	10.1	8.23	8.68	9.18	9.71	9.20
Mo	67.5	62.8	60.4	48.3	57.7	59.3	56.0	49.5	44.2	47.9	53.7	50.3	53.0
Ba	371	363	337	321	338	344	330	319	287	360	350	340	340
Hf	3.64	3.88	3.97	3.70	4.24	4.20	4.01	3.85	3.32	3.60	3.67	3.80	3.76
Ta	0.74	0.75	0.69	0.82	0.80	0.70	0.68	0.66	0.64	0.57	0.60	0.64	0.61
Pb	58.6	55.2	44.8	36.1	40.5	41.4	38.8	36.9	34.3	38.6	41.6	40.6	39.8
Th	21.1	19.8	16.6	12.2	13.0	12.5	11.9	11.3	9.80	9.93	10.7	10.6	10.1
U	3.82	4.76	5.90	4.75	4.89	4.76	4.25	3.95	3.41	3.63	3.67	3.40	3.32

Table 2. (continued)

PC05	PC05	PC05	PC05	PC05	PC05	PC05	PC05	PC05	PC05	PC05	PC05	PC05	PC05	PC05
9	9	9	10	10	10	10	11	11	11	11	12	12	12	12
72–74	82–84	92–94	22–24	32–34	72–74	82–84	22–24	32–34	72–74	82–84	22–24	32–34	72–74	82–84
7.96	8.06	8.16	8.46	8.56	8.96	9.06	9.45	9.55	9.95	10.05	10.45	10.55	10.95	11.05
49.7	50.8	50.5	52.3	53.8	52.5	54.0	53.4	54.6	52.0	54.4	52.8	54.4	53.8	54.6
0.51	0.50	0.50	0.54	0.54	0.57	0.57	0.58	0.60	0.58	0.55	0.53	0.56	0.65	0.61
14.1	14.1	13.9	14.9	14.9	15.0	15.3	15.0	15.4	14.8	15.1	15.1	15.2	15.4	15.2
5.17	5.31	5.13	5.60	5.71	5.91	5.97	5.86	6.05	6.22	5.50	5.18	5.41	5.94	5.63
1.71	1.78	1.43	1.28	1.31	1.16	1.24	1.30	1.22	1.95	1.70	1.62	1.63	1.50	1.76
2.82	2.78	2.84	3.20	3.09	3.13	3.19	3.08	3.18	3.15	2.99	2.83	2.98	3.14	2.88
5.38	5.38	6.01	3.32	3.15	2.82	2.39	2.52	1.96	2.65	2.28	2.55	2.33	1.77	2.23
3.88	3.49	3.39	3.64	3.28	3.88	3.49	3.48	3.37	3.62	3.43	3.57	3.38	3.36	3.32
4.52	4.35	4.12	4.27	4.13	4.28	4.10	3.96	4.17	4.25	4.51	4.67	4.53	4.29	4.42
3.36	3.37	3.90	1.95	1.89	1.46	1.36	1.48	1.07	1.47	1.27	1.47	1.31	0.90	1.24
8.86	8.17	8.28	9.02	8.19	9.28	8.44	9.43	8.35	9.30	8.24	9.63	8.21	9.20	8.12
100	100	100	100	100	100	100	100	100	100	100	100	100	100	100
172	221	252	116	142	153	142	218	149	195	155	160	154	117	155
140	194	200	122	170	161	170	193	170	186	174	149	167	153	175
48.8	64.5	73.2	34.3	41.6	42.9	43.0	66.6	47.7	52.1	45.8	42.2	45.6	33.4	46.4
200	269	304	140	174	174	180	279	199	211	193	173	189	134	193
47.1	63.1	70.6	33.0	40.5	40.3	41.8	64.4	46.6	49.1	45.2	39.9	44.2	31.2	44.6
11.6	15.5	17.4	7.96	9.75	9.83	10.0	15.4	11.0	11.9	10.7	9.69	10.4	7.41	10.7
54.2	69.8	79.5	36.9	44.3	44.3	44.3	68.4	48.8	55.6	48.9	45.1	47.9	33.4	48.3
8.11	10.4	12.0	5.46	6.67	6.56	6.66	10.1	7.28	8.36	7.36	6.77	7.18	5.00	7.27
51.6	66.1	76.0	34.0	41.7	40.8	41.2	60.7	43.9	52.3	45.4	43.0	44.8	30.0	44.8
10.9	13.6	15.8	6.97	8.59	8.22	8.22	11.8	8.51	10.7	9.22	8.95	9.07	5.97	8.99
31.5	38.8	45.1	20.1	24.6	23.3	23.2	31.9	23.0	30.3	25.9	26.2	25.8	16.4	24.9
4.41	5.34	6.21	2.79	3.44	3.17	3.14	4.19	2.99	4.13	3.54	3.70	3.58	2.22	3.38
27.6	32.9	38.5	17.7	21.4	19.7	19.2	24.7	17.9	25.4	21.4	23.6	22.0	13.8	20.4
4.16	4.94	5.85	2.64	3.26	2.90	2.85	3.53	2.58	3.69	3.19	3.57	3.35	1.99	3.07
308	415	483	197	257	241	240	350	236	317	267	275	267	166	255
1120	1484	1680	776	989	972	976	1403	1013	1213	1055	1009	1041	751	1041
620	828	918	453	577	582	587	837	622	706	624	573	611	476	625
501	657	762	323	411	390	389	566	391	507	432	436	431	274	416
0.35	0.37	0.34	0.44	0.50	0.45	0.50	0.37	0.46	0.42	0.47	0.42	0.46	0.56	0.47
32.2	48.0	50.6	30.3	37.1	36.0	35.7	45.2	39.9	40.8	38.9	39.7	39.9	33.2	33.8
97.4	104	94.0	90.9	97.8	96.1	101	146	107	112	104	97.0	106	113	111
21.7	23.3	22.8	24.7	28.4	25.1	26.6	46.0	30.4	35.5	29.2	23.4	29.4	28.6	26.3
137	156	135	100	127	107	110	131	113	189	154	158	162	134	161
427	467	365	229	282	311	285	442	304	654	375	377	363	393	399
348	377	330	272	312	288	286	404	285	388	324	325	323	297	297
154	159	173	170	193	190	182	194	184	209	194	186	189	200	184
66.4	86.8	86.5	77.4	98.6	103	101	118	107	103	100	95.8	103	111	106
212	306	313	143	206	186	187	224	182	216	220	175	210	169	215
109	145	146	106	142	139	144	151	152	145	148	126	153	156	153
6.60	8.71	9.32	8.26	10.3	10.5	10.9	12.7	12.0	11.3	11.5	10.5	12.1	13.8	13.4
43.9	55.2	38.4	22.0	30.2	27.8	31.0	36.2	29.3	54.3	40.1	36.4	38.0	30.1	39.7
319	341	314	266	331	346	318	360	348	470	382	348	389	439	436
2.93	3.77	3.71	2.93	3.81	3.59	3.94	3.85	4.22	3.80	4.03	3.45	4.09	3.93	4.24
0.54	0.58	0.62	0.69	0.70	0.70	0.73	0.75	0.80	0.69	0.76	0.77	0.81	0.95	0.91
35.0	43.5	34.9	27.2	34.5	32.1	35.3	39.3	36.9	46.5	40.5	36.7	39.0	34.5	41.2
7.47	9.67	12.2	9.59	11.3	10.6	10.6	14.5	12.8	12.2	12.3	10.8	12.5	12.2	12.9
2.93	3.37	3.76	2.02	2.37	1.99	2.01	2.21	1.93	2.13	2.02	2.03	2.11	1.87	2.15

2b). Scattered ferromanganese micronodules (<1 mm) are highly abundant from the core top to 0.7, 2.3 to 3.6, and 9.8 to 10.0 mbsf, and moderately abundant from 0.7 to 1.2 and 6.5 to 7.0 mbsf. The sediment is moderately bioturbated from the core top to 0.7, 3.6 to 3.9, 7.4 to 8.3, and 9.9 mbsf to the core bottom. Lighter colored lenses, broken by darker colored burrows, are abundant in these intervals, except in core top to 0.7 mbsf. The sediment is slightly bioturbated in depths 0.7 to 1.0, 2.2 to 2.4, 3.4 to 3.6, 8.4 to 9.0, and 9.4 to 9.8 mbsf.

Radiolarian tests are few and diatoms are absent in these cores. In addition, there are neither calcareous microfossils nor key beds such as tephra layers. Thus, the ages of the sediments are uncertain.

We analyzed the major element, trace element, and REY composition of 149 bulk sediment samples: 63 samples from PC04 and 86 from PC05. Major element content was determined by X-ray fluorescence spectrometry, and trace element and REY abundances were measured by inductively coupled plasma mass spectrometry, both undertaken at the University of Tokyo. Sample preparation and analytical procedures are described by Fujinaga *et al*. (2016).

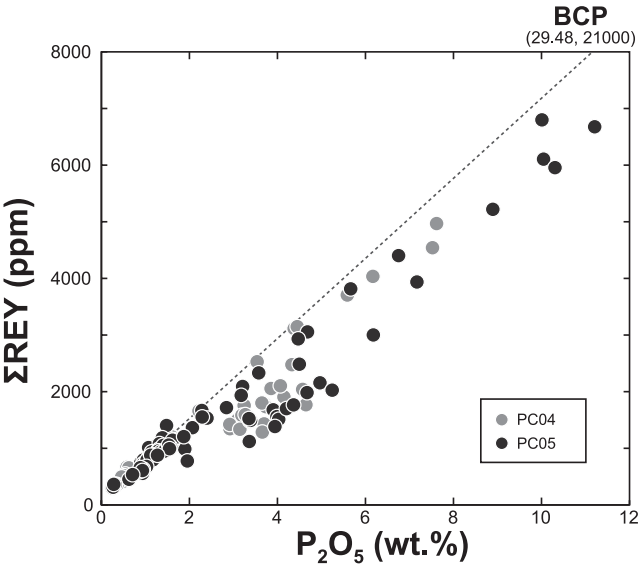

Fig. 3. P_2O_5 versus ∑REY content of bulk samples from PC04 and PC05. Composition of biogenic calcium phosphate (BCP) is from Kon et al. (2014).

Results and Discussion

Bulk chemical compositions of all samples from PC04 and PC05 are given in Tables 1 and 2, respectively. Bulk ∑REY content in PC04 and PC05 varied considerably downhole (Fig. 2). The most prominent feature of the profiles is the presence of layers with anomalously high ∑REY content. The maximum ∑REY content in PC04 is almost 5000 ppm at 8.29 mbsf; a ~0.8 m-thick layer contains more than 2000 ppm of ∑REY. The maximum ∑REY content in PC05 is 6800 ppm at 2.97 mbsf; a ~1.0-m-thick layer contains more than 2000 ppm of ∑REY. At 6.87 mbsf, PC05 also has a minor peak of ∑REY with 3000 ppm and a ~0.4-m-thick layer with more than 2000 ppm.

Kato *et al*. (2011) originally defined REY-rich mud as deep-sea sediment with ∑REY > 400 ppm, which was based on a typical grade of ion-adsorption-type REY deposits on land (Bao and Zhao, 2008). Considering the anomalously high ∑REY content of the REY-rich mud within the Minamitorishima EEZ, we classify REY-rich mud here on the basis of bulk ∑REY content as follows: 400–2000 ppm ∑REY is "REY-rich mud," 2000–5000 ppm ∑REY is "highly REY-rich mud," and >5000 ppm ∑REY is "extremely REY-rich mud."

The downhole variation of ∑REY in PC04 shows that the sediment from the core top to 1.35 mbsf contains less than 400 ppm ∑REY (Fig. 2a). From 1.35 to ~7.0 mbsf, bulk ∑REY content is moderate (400–670 ppm), followed by a continuous rise in ∑REY toward the peak at 8.29 mbsf (Fig. 2a). The interval between 7.79 and 8.57 mbsf corresponds to the highly REY-rich mud. Below the peak horizon, ∑REY content rapidly decreases to ~1500 ppm and varies mainly within the relatively high ∑REY range of 1500–2000 ppm from 8.67 mbsf to the core bottom.

The surface sediment in PC05 between the core top and 0.23 mbsf contains less than 400 ppm ∑REY (Fig. 2b). From 0.60 to 2.47 mbsf, the sediment is categorized as REY-rich mud, with an increasing trend of ∑REY content from ~2 mbsf. The interval between 2.57 and 2.87 mbsf corresponds to the highly REY-rich mud. Below this, between 2.97 and 3.37 mbsf, is the extremely REY-rich mud showing maximum ∑REY content of 6800 ppm at 2.97 mbsf (Fig. 2b). The interval between 3.47 and 3.57 mbsf consists of the highly REY-rich mud again. Below the most REY-enriched layer, bulk ∑REY content changes mainly within a range of 700 and 1400 ppm between ~3.9 and 6.5 mbsf. The second REY-enriched horizon occurs in the interval between 6.57 and 7.17 mbsf with peak ∑REY content of 3000 ppm, followed by relatively high ∑REY content around 1500 ppm up to 8.16 mbsf. Below 8.46 mbsf, ∑REY content slightly decreases to 750–1200 ppm.

In both cores, the highly and the extremely REY-rich muds are characterized by abundant large grains of phillipsite and BCP. There is a distinct positive correlation between P and ∑REY content in both cores (Fig. 3), which is consistent with previous observations that BCP is the main host phase of REY in deep-sea sediments (Toyoda *et al*., 1990; Kashiwabara *et al*., 2014; Kon *et*

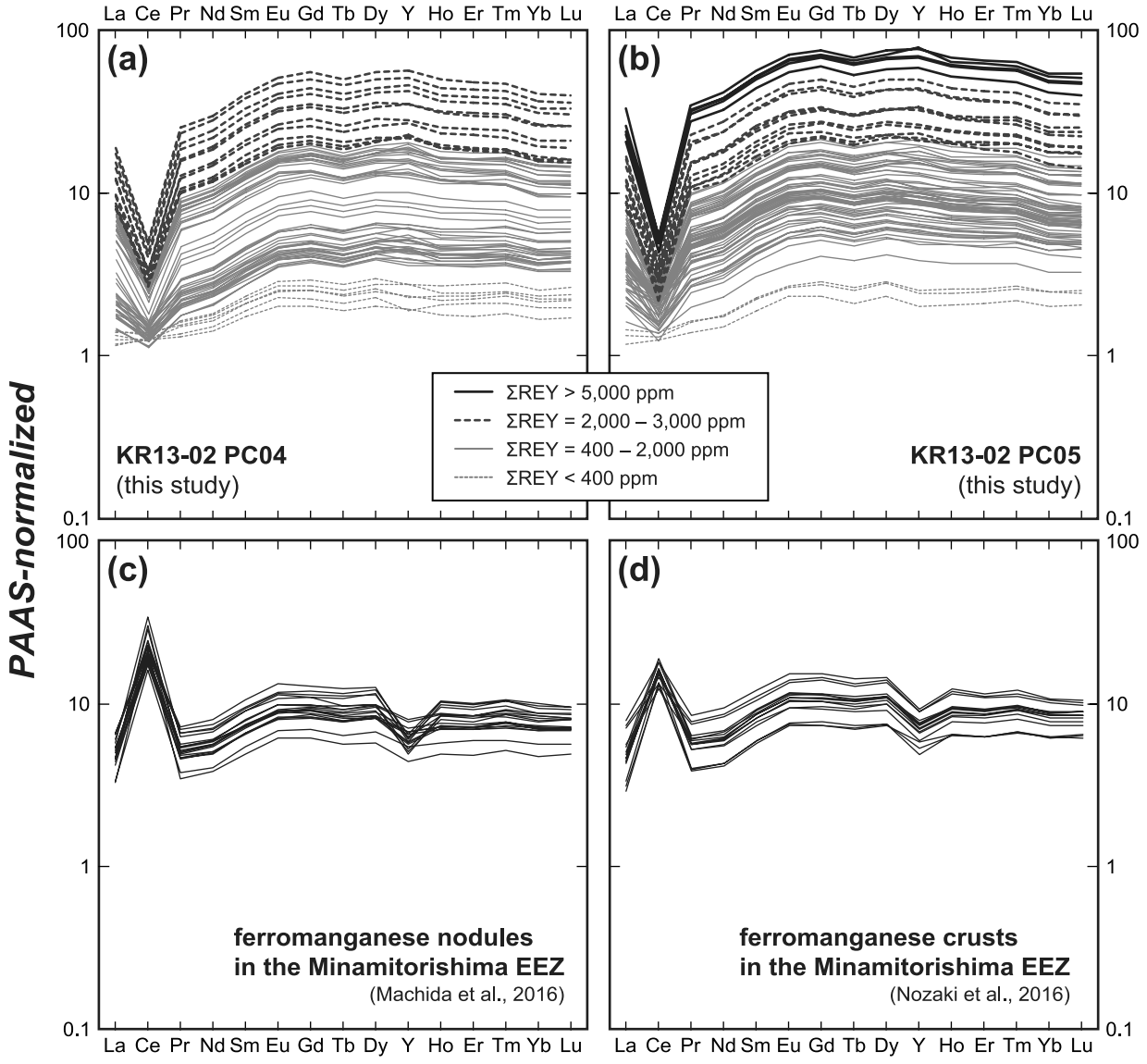

Fig. 4. Spider diagrams showing REY patterns of bulk samples from PC04 and PC05 in Figs. 2 and 3, ferromanganese nodules in the Minamitorishima EEZ (Machida et al., 2016), and ferromanganese crusts in the Minamitorishima EEZ (Nozaki et al., 2016), all normalized with respect to PAAS (Taylor and McLennan, 1985).

al., 2014). Detailed grain-size distributions of these cores are discussed by Ohta *et al*. (2016).

We compared the REY patterns of bulk sediments normalized with respect to post-Archean average Australian shale (PAAS; Taylor and McLennan, 1985), a representative index of the upper continental crust (Figs. 4a and 4b). The highly and extremely REY-rich muds contain between 15 and 30 times more ∑REY on average than the PAAS. More importantly, heavy rare-earth elements (HREE; here defined as Eu to Lu, following Kato *et al*., 2011) in highly REY-rich mud are 30 times more concentrated on average than in PAAS. Furthermore, average content of total HREE (∑HREE) in extremely REY-rich mud reaches almost 60 times higher than that in PAAS. Another obvious feature is the variation in the magnitude of the Ce anomaly (Ce/Ce*; Tables 1 and 2). The surface sediments showing no REY enrichment exhibit almost no Ce anomaly (Ce/Ce* = 0.9–1) with relatively flat REY patterns as a whole (Figs. 4a and 4b). With increasing bulk ∑REY content, the negative Ce anomaly increases (Figs. 4a and 4b), corresponding to a decrease in Ce/Ce* to ~0.2.

Samples of ferromanganese nodules (Machida *et al*., 2016) and crusts (Nozaki *et al*., 2016) collected from the eastern and southern Minamitorishima EEZ have ∑REY concentrations, excluding Ce, 4–8 times and 4–9 times

higher than PAAS, respectively (Figs. 4c and 4d). In addition, ∑HREE content of ferromanganese nodules and crusts is 6–12 times and 7–13 times that of PAAS, respectively. Ion-adsorption-type REY deposits in southern China, which dominate world HREE production, have ∑HREE content of 50–200 ppm (Bao and Zhao, 2008), or 3–11 times that of PAAS. The ∑REY and ∑HREE concentrations of the highly and the extremely REY-rich muds are more than ten times higher than those of the Chinese deposit. Moreover, it has been demonstrated that leaching of these mud samples with dilute acid (0.5 mol/L HCl) successfully extracted about 90% of the REY (except for Ce) (Takaya *et al*., 2015). Thus the extraordinary REY content and ease of REY extraction from the highly and the extremely REY-rich muds suggests that they represent a promising novel REY resource.

Conclusions

We confirmed the presence of deep-sea REY-rich mud in the Minamitorishima EEZ. Our analysis of two sediment cores demonstrates the highest REY concentration measured on the modern sea floor. These highly and extremely REY-rich muds are present as ~1 m-thick stratigraphic layers. The muds contain abundant phillipsite and BCP, and show a relatively homogeneous texture. The peak ∑REY content in KR13-02 cores PC04 and PC05 is ~5000 ppm and ~7000 ppm, respectively. PC04 has a single peak horizon of ∑REY, and PC05 has two peak horizons, although the second peak is relatively minor (at most ~3000 ppm). Of particular note, the average ∑HREE content in extremely REY-rich mud reaches almost 60 times that of average shale. Considering that these highly and extremely REY-enriched layers occur at depths shallower than 10 m below the seafloor, and that most of REY in the muds can be easily leached, these muds might provide a solution for the predicted substantial growth of global REY demand in the near future.

Acknowledgments—This research was supported by JSPS through Grants-in-Aid Scientific Research (S) No. 22226015 and No. 15H05771 to Y.K. and (B) No. 25289334 to K.N. We thank Y. Itabashi and C. Kabashima for their assistance with sample preparations and chemical analysis. We greatly appreciate Y. Watanabe and P. Emsbo for their constructive reviews that have considerably improved the manuscript. We are obliged to J. Ishibashi for his careful handling of the manuscript.

References

Alonso, E., Sherman, A. M., Wallington, T. J., Everson, M. P., Field, F. R., Roth, R. and Kirchain, R. E. (2012) Evaluating rare earth element availability: A case with revolutionary demand from clean technologies. *Environ. Sci. Technol. Lett*. **46**, 3406–3414.

Bao, Z. and Zhao, Z. (2008) Geochemistry of mineralization with exchangeable REY in the weathering crusts of granitic rocks in South China. *Ore Geol. Rev*. **33**, 519–535.

Fujinaga, K., Yasukawa, K., Nakamura, K., Machida, S., Takaya, Y., Ohta, J., Araki, S., Liu, H., Usami, R., Maki, R., Haraguchi, S., Nishio, Y., Usui, Y., Nozaki, T., Yamazaki, T., Ichiyama, Y., Ijiri, A., Inagaki, F., Machiyama, H., Iijima, K., Suzuki, K., Kato, Y. and KR13-02, MR13-E02 Leg 2 and KR14-02 Cruise Members (2016) Geochemistry of REY-rich mud in the Japanese Exclusive Economic Zone around Minamitorishima Island. *Geochem. J*. **50**, this issue, 575–590.

Kashiwabara, T., Toda, R., Kato, Y., Fujinaga, K., Takahashi, Y. and Honma, T. (2014) Determination of host phase of lanthanum in deep-sea REY-rich mud by XAFS and μ-XRF using high-energy synchrotron radiation. *Chem. Lett*. **43**, 199–200.

Kato, Y., Fujinaga, K., Nakamura, K., Takaya, Y., Kitamura, K., Ohta, J., Toda, R., Nakashima, T. and Iwamori, H. (2011) Deep-sea mud in the Pacific Ocean as a potential resource for rare-earth elements. *Nat. Geosci*. **4**, 535–539.

Kato, Y., Fujinaga, K., Takaya, Y., Nakamura, K. and Iwamori, H. (2012) Is deep-sea mud a promising resource for rare-earth elements? (abstract). *Abstracts with Programs, the Society of Resource Geology* **62**, 37.

Kon, Y., Hoshino, M., Sanematsu, K., Morita, S., Tsunematsu, M., Okamoto, N., Yano, N., Tanaka, M. and Takagi, T. (2014) Geochemical characteristics of apatite in heavy REE-rich deep-sea mud from Minamitorishima area, southeastern Japan. *Resour. Geol*. **64**, 47–57.

Machida, S., Fujinaga, K., Ishii, T., Nakamura, K., Hirano, N. and Kato, Y. (2016) Geology and geochemistry of ferromanganese nodules in the Japanese Exclusive Economic Zone around Minamitorishima Island. *Geochem. J*. **50**, this issue, 539–555.

Marsaglia, K., Milliken, K. and Doran, L. (2013) Smear slides of marine mud for IODP core description, Volume I. Part 1: Methodology and atlas of siliciclastic and volcanogenic components. *IODP Technical Note 1*, doi:10.2204/iodp.tn.1.2013.

Marsaglia, K., Milliken, K., Leckie, R., M., Tentori, D. and Doran, L. (2015) IODP smear slide digital reference for sediment analysis of marine mud. Part 2: Methodology and atlas of biogenic components. *IODP Technical Note 2*, doi:10.14379/iodp.tn.2.2015.

Nakamura, K., Machida, S., Okino, K., Masaki, Y., Iijima, K., Suzuki, K. and Kato, Y. (2016) Acoustic characterization of pelagic sediments using sub-bottom profiler data: Implications for the distribution of REY-rich mud in the Minamitorishima EEZ, western Pacific. *Geochem. J*. **50**, this issue, 605–619.

Nozaki, T., Tokumaru, A., Takaya, Y., Kato, Y., Suzuki, K. and Urabe, T. (2016) Major and trace element compositions and resource potential of ferromanganese crust at Takuyo Daigo Seamount, northwestern Pacific Ocean. *Geochem. J*. **50**, this issue, 527–537.

Ohta, J., Yasukawa, K., Machida, S., Fujinaga, K., Nakamura, K., Takaya, Y., Iijima, K., Suzuki, K. and Kato, Y. (2016) Geological factors responsible for REY-rich mud in the

western North Pacific Ocean: Implications from mineralogy and grain size distributions. *Geochem. J.* **50**, this issue, 591–603.

Takaya, Y., Fujinaga, K., Yamagata, N., Araki, S., Maki, R., Usami, R., Nakamura, K. and Kato, Y. (2015) Chemical leaching of rare earth elements from highly REY-rich mud. *Geochem. J.* **49**, 637–652.

Taylor, S. R. and McLennan, S. M. (1985) The *Continental Crust: Its Composition and Evolution*. Blackwell Scientific Publications, Oxford, 312 pp.

Toyoda, K., Nakamura, Y. and Masuda, A. (1990) Rare earth elements of Pacific pelagic sediments. *Geochim. Cosmochim. Acta* **54**, 1093–1103.

Supplementary Materials

URL (http://www.terrapub.co.jp/journals/GJ/archives/data/50/MS431.pdf)
Figure S1